
Article:
Williams, D., Copley, R., Bugryniec, P. et al. (2 more authors) (2024) A review of ultrasonic monitoring: assessing current approaches to Li-ion battery monitoring and their relevance to thermal runaway. Journal of Power Sources, 590. 233777. ISSN 0378-7753

https://doi.org/10.1016/j.jpowsour.2023.233777

Journal of Power Sources 590 (2024) 233777

Contents lists available at ScienceDirect

Journal of Power Sources

journal homepage: www.elsevier.com/locate/jpowsour

Review article

A review of ultrasonic monitoring: Assessing current approaches to Li-ion battery monitoring and their relevance to thermal runaway

Daniel Williams [a], Royce Copley [a], Peter Bugryniec [b], Rob Dwyer-Joyce [a], Solomon Brown [b,*]

[a] Department of Mechanical Engineering, Engineering Heartspace, Sir Frederick Mappin Building, Mappin Street, S1 3JD, UK
[b] Department of Chemical & Biological Engineering, The University of Sheffield, Mappin Street, Sheffield, S1 3JD, UK

GRAPHICAL ABSTRACT

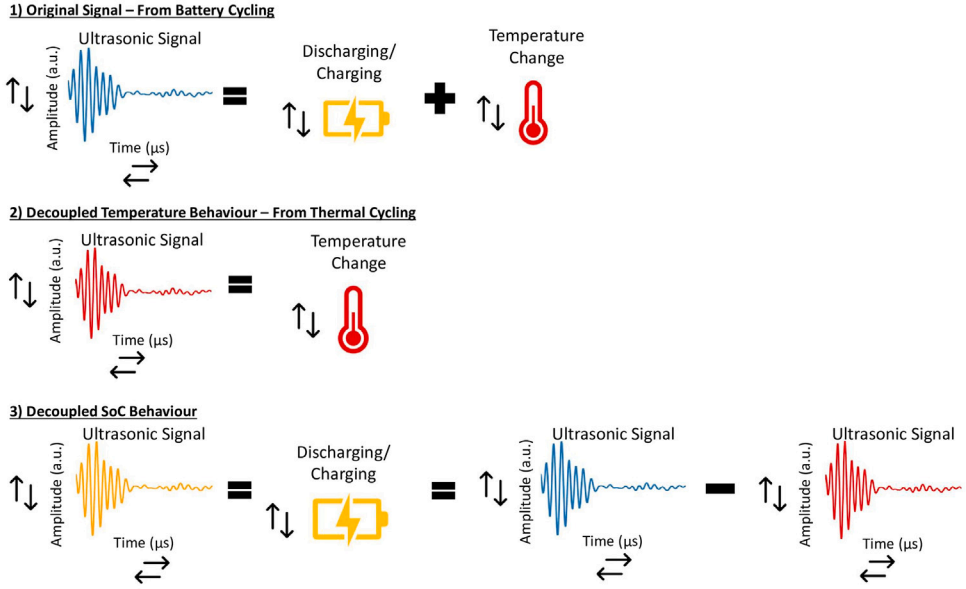

HIGHLIGHTS

- Review of state-of-charge and state-of-health monitoring using ultrasound.
- Literature focuses on detecting internal changes related to defects and charge.
- Need to investigate correlation between ultrasonic signal and thermal runaway onset.
- Decoupling temperature and charge effects in the ultrasonic signal is required.

ARTICLE INFO

Keywords:
Acoustic monitoring
Calibration

ABSTRACT

Li-ion batteries (LIBs) are increasingly used in applications from personal electronics to electric vehicles (EVs) and grid scale storage. Research into LIB monitoring, such as state-of-charge (SOC) and state-of-health (SOH), and the effects of abuse on LIBs has received increased attention to allow for better battery performance

* Correspondence to: Department of Chemical and Biological Engineering, Room C04 Pam Liversidge Building, Mappin Street, Sheffield S1 3JD, UK.
E-mail address: s.f.brown@sheffield.ac.uk (S. Brown).

https://doi.org/10.1016/j.jpowsour.2023.233777
Received 13 June 2023; Received in revised form 16 October 2023; Accepted 23 October 2023
Available online 2 November 2023

Time-of-flight
Thermal effects
Diagnostics

and safety. To improve LIB safety better detection of thermal runaway (TR) is required for the mitigation of the associated consequences or to prevent it entirely. This paper reviews the growing field of ultrasound (US) sensing of LIBs for state monitoring and thermal runaway detection, with an additional perspective on of advancements made in thermal runaway testing. In this work, US is categorised by: hardware used in research; application for SOC and SOH monitoring. Further, TR is categorised by abuse scenario: overheating; penetration; overcharging; and gas generation. This review summarises the development of US to detect changes within a LIB. However, it is found that further developments are required to (1) isolate and characterise the various abuse/failure mechanisms using US and (2) decouple temperature and charge effects on the US signal. It is shown that decoupling the temperature-charge relationship within the US signal is necessary for accurate SOC and SOH monitoring.

Nomenclature

Abbreviations

ARC	Accelerated rate calorimeter
LIBs	Li-ion batteries
EV	Electric vehicle
TR	Thermal runaway
BMS	Battery management system
SOC	State of charge
SOH	State of health
US	Ultrasound/ultrasonic
NMC	Lithium-nickel-manganese-cobalt-oxide
NCA	Lithium-nickel-cobalt-aluminium-oxide
LFP	Lithium-iron-phosphate
LMP	Lithium-manganese-phosphate-oxide
OCV	Open circuit voltage
SEI	Solid-electrolyte interface
ToF	Time-of-flight
SOS	State of safety
AScan	Amplitude scan
LMP	Lithium-manganese-iron-oxide $LiMnPO_4$
HWS	Heat-wait-seek
C-rate	Coulomb rate
CC-CV	Constant-current-constant-voltage

Units

V	Volts
°C	Degree Celsius
J g^{-1}	Joules per gram
m s^{-1}	metres per second
Pa	Pascal
kg m^{-3}	Kilogrammes per cubic metre
Pa s m^{-3}	Pascal second per cubic metre
Hz	Hertz
s	Seconds

Variables

c	Speed of sound (m s^{-1})
E	Young's modulus (MPa)
rho	Density (kg m^{-3})
z	Acoustic impedance (P m^{-3})
R	Reflection coefficient

1. Introduction

Within the last few decades, Li-ion batteries (LIBs) have seen a surge in popularity and application from personal electronics to the electric vehicle (EV) market and large scale energy storage [1–3]. With this increase in demand, investment in the LIB sector is expected to grow by 22% by 2030. The growth is driven, in part, by their high energy density, long cycle life, low self discharge and high power output making them an ideal energy storage device for electrical applications [4,5]. However, there are several limitations that are associated with LIBs, including: over-charging; thermal runaway; dendritic lithium; current collector dissolution and gas evolution [6]. These limitations can damage the cells by: reducing available lithium or electrode; creating internal stress; causing short circuiting; and potentially leading the cell to catch fire or explode. This leads to a need for more sophisticated diagnostic systems; specifically, monitoring of LIBs for detection of thermal runaway (TR).

LIBs pose safety risks due to the combustible materials and oxidising agents that coexist within them. These properties can cause runaway reactions during abusive use, and can lead to fires and explosions. Battery abuse can be divided into three categories: (i) mechanical abuse; (ii) thermal abuse and; (iii) electrical abuse [7–9]. Thermal abuse is the overheating of a cell, either from external factors or internal heat generation. Electrical abuse is due to short-circuiting, over-charging or over-discharging in the battery. Mechanical abuse is the deformation of the battery due to external forces; this could be caused by piercing or crushing the battery, causing a short circuit within the battery.

As a result of these risks, a battery management system (BMS) is implemented to carefully monitor various states of the battery, such as the state-of-charge (SOC) or state-of-health (SOH). There are multiple methods employed by BMSs, which vary in benefits and drawbacks and will be described. A recently proposed method of monitoring LIBs is ultrasonic (US) monitoring, which can provide information on changes within the battery, such as gas generation, SOC and lithium plating [10,11].

As US monitoring of LIBs is a new development, focus has been placed on the efficacy of the method; specifically, on the detection of SOC and SOH. An area of research that can further progress the use of US monitoring is the viability of monitoring abuse conditions, leading to TR detection. As such, understanding how variables such as temperature, charge and failure modes affect the US signal should be focused on.

The aim of this paper is to review current literature on US monitoring of LIBs, discuss the advantages and flaws of current techniques and make recommendations to enable the practical application of LIB monitoring. To do so, the paper is split into three sections. Section 2 provides: an overview of the safe operation of LIBs; an introduction into current battery management systems; and the theory of ultrasonic testing. Section 3 draws together existing literature into three sections: 3.1 focuses on the current use of US for SOC and SOH and its applicability to the detection of thermal runaway; Section 3.2 focuses abuse mechanisms of thermal runaway in LIBs and how the chemistry and charge/charge rate have an effect; and Section 3.3 takes a look at the application of US to monitor abuse conditions of LIBs. The paper concludes with Section 4, outlining recommendations on what needs to be addressed – and how to address these aspects – in order to improve viability of US monitoring of LIBs in practical applications.

2. Background of key concepts

In this section, 2.1 introduces LIBs, the safe operating conditions, what happens outside the safe operating range; what factors are monitored to prevent unsafe operation. Section 2.2 introduces BMSs, the SOC estimation methods used and the categorisation of said estimation methods. Section 2.3 defines the theory of US monitoring and explains the mechanics that allow for US monitoring of LIBs.

2.1. Li-ion battery safe operation

LIBs are primarily used due to their high energy density, high power density and long cycle life compared to other common battery types [12,13]. There are various cathode materials that LIBs can utilise e.g., NMC (lithium-nickel-manganese-cobalt-oxide), NCA (lithium-nickel-cobalt-aluminium-oxide), LFP (lithium-iron-phosphate). LIBs can also have different electrolytes, material structures and cell construction. The combinations of these materials affect various battery properties, such as energy density, life cycle, specific power, and safety.

One major restriction with LIBs is the small range for safe operation – for both voltage and temperature – restricting use in more variable climates and work conditions. For voltage, the safe operating range is between 1.5–4.2 V, depending on the cathode material. The safe operating temperatures can range from 0 to 45 °C and from −20 to 55 °C when charging and discharging, respectively [12]. When the battery reaches a temperature of 90 °C, the solid electrolyte interface (SEI) begins to break down. The SEI has two important roles: (i) protection against graphite co-intercalating with electrolyte solvent molecules and; (ii) prevention of Li-ions consumption [14]. At higher temperatures, the SEI film is unable to prevent lithiated anode–electrolyte reactions, generating gases [15].

In contrast, when a battery is operating at lower temperatures, the anode undergoes increased polarisation [16]. The increased polarisation induces lithium plating before complete lithiation can occur. If the SEI is fragile, deposited lithium-ions can grow from the plating to form lithium dendrites [17]. These dendrites can result in increased risk of short circuiting [18] and thermal runaway due to decreased SEI stability [17].

Over-charging can cause lithium dendrite formation, which can pierce the separator. This can lead to the battery short-circuiting, causing a positive feedback loop in temperature rise leading to thermal runaway. At lower temperatures, the cathode can undergo short circuiting. When the minimum voltage drops below 1.5 V, when the first derivative of the voltage is 0, the copper in the current collector foil begins to oxidise followed by the dissolution of the copper after the cathode breaks down. The dissolution can lead to capacity loss, as well as the deposition of the copper on the anode, cathode and cathode-facing separator surfaces. [19,20].

Battery abuse can be categorised into three main groups: mechanical abuse, electrical abuse and thermal abuse [15,21]. Along with latent defects inside the battery, these abuse mechanics can lead to thermal runaway, resulting in battery failure, smoke, and fire or explosion [22]. In order to reduce the risk of TR, the SOC of a cell is monitored; preventing the cell from over- or under-charging thus reducing the risk of electrical abuse. The SOC is defined as the percentage of the maximum possible charge remaining in the battery [23] where 100% SOC is fully charged and 0% is fully discharged. Although this definition is straightforward, calculating the SOC is complex.

There are multiple reasons for the complexity of estimating the SOC: the maximum possible capacity, Q_{max}, decreasing throughout the lifespan of the battery; the capacity being affected by the ambient temperature and age of the battery [24]; and the requirements of parameters such as the initial SOC and impedance [25].

In order to combat the difficulties of estimating the SOC, BMSs have been developed. As a result of the complexity, different methodologies have been employed in BMS development along with the implementation of different theories [26]. These variations are discussed and elaborated upon in the following section.

2.2. Battery management systems

A BMS is a system that monitors the states and parameters of the battery pack, which include cell voltage, current, temperature; as well as calculate the SOC and SOH of the pack [27]. The BMS uses these parameters as inputs to determine, amongst other operational criteria, when to limit dis/charging and to shut down operation of the battery to prevent it being damage or undergoing TR. Here we will focus on SOC and SOH estimation methods.

According to How et al. [28], there are two established categories and three relatively new categories for classifying SOC estimation methods. The two established methods are: model-based estimation using electrical, chemical or a combination of those properties for individual batteries, based on the porous electrode theory and; data-driven estimation measuring the change in battery parameters. The three new categories are: look-up table estimation which exploits the direct mapping relationship between SOC and external characteristics, such as open-circuit voltage; Coulomb counting estimation that measures and integrates the discharging current over time; and a hybrid method using a combination of usually two or three algorithms. These five methods will be briefly covered in this review. Core comprehensive review of current BMSs have been performed by How et al. [28] and Wang et al. [29].

Model-based approaches utilise different theories to model the chemical or electrical parameters of a specific battery. Electrochemical models are based on the porous electrode theory [30] and utilise partial differential equations [28]. Equivalent circuit models, such as the Thevenin model [31], utilises the open-circuit voltage, ohmic internal resistance and RC networks (polarisation internal resistance and internal capacitance) to model a battery [32]. Electrochemical impedance models build on equivalent circuit models by including more parameters and theories, including the Warburg element and Z_{arc} element [33,34].

Data driven methods measure parameters such as voltage, current and temperature in order to estimate battery SOC [35] utilising machine learning algorithms. Commonly used methods include neural networks, deep learning — neural networks with multiple hidden layers [36], support vector machines and fuzzy logic [28]. These methods differ from model-based as they do not require human input other than the datasets.

Coulomb counting estimates the SOC by integrating the current of the battery over time. This means the estimation is specific to the battery in question. This is the most favourable method due to its simplicity [37]. Since integration is utilised, a small error can become substantial due to the compounding of the error. To account for this, an operating coefficient η_i is considered [38]. Look-up tables exploit the relationship between SOC and numerous external battery parameters such as impedance and open-circuit voltage, based on the tabulations of relationships through experimentation [39].

There are other ways of classifying BMS estimation methods. One such classification, defined by Berecibar et al. [40], employs two categories: experimental techniques and adaptive models, as shown in Table 1. Experimental techniques compare cycling data history of an active battery to that of previous batteries, to extract SOH estimations. This is limited by cell chemistry, design and operating conditions, reducing the transferability of the knowledge across multiple batteries. This approach also requires an understanding of the relation between degradation and operation, obtained by evaluation of large datasets or physical analysis of the cell.

Adaptive models can quantify degradation based on parameters that are affected by said degradation. The parameters must be measurable or should be examined in the cell throughout the cell operation. This reduces the number of tests required to accurately monitor the cell, as well as allow greater adaptability across different cell chemistries and form factors [12]. There exists a trade-off between accuracy and computational power. The most accurate methods for experimental

Table 1
Benefits and drawbacks of the established state-of-charge estimation methods.
Source: Reproduced from [40].

	Experimental techniques	Adaptive methods
Based on	Storing the lifetime data and the use of the previous knowledge of the operation performance of the cell/battery.	Calculation of the parameters, which are sensitive to the degradation in a cell/battery.
Advantages	1. Low computational effort 2. Possible implementation in a BMS	1. High accuracy 2. Possible to be used as in-situ estimation
Disadvantages	1. Low accuracy 2. Not suited for in-situ estimation	1. High computational effort 2. Difficult in BMSs implementation

techniques are impedance measurement and sample entropy. However Coulomb counting and the probabilistic methods are the most common due to their simplicity.

Many BMS estimation methods have an estimation error in the range of > 1%–12%, with the most common being reported between 5%–10%. There are some simple methods that can provide accurate results such as Coulomb counting [38] and open circuit voltage (OCV) methods [41]. However, these low error ranges are obtained if the battery is in a stable state and with a low variance of battery parameters. For accurate measurements in unstable states, more complex methods are required [42] Some complex models include: Kalman filtering [43]; particle filtering [44]; and Gaussian process functional regression [45].

Sophisticated estimation methods have been recently developed using neural networks, due to the limited improvement provided by simple BMSs. Multiple safety incidents in LIBs have occurred when simple BMSs have been used, and the lifespan of a battery pack is noticeably less than an individual cell [46]. More sophisticated BMSs provide better protection against over-charge and over-discharge, improving lifespan and safe usage of batteries.

Many of these methods utilise battery parameters that are externally measured – such as current, temperature and ohmic resistance – to monitor a battery [47]. As a result, recent interest in ultrasound as a supplementary method for BMSs has been explored. Ultrasound is suggested to detect internal changes to the cell which would be used to estimate the SOC. In the following section, the mechanics of ultrasound is explained and how it is applicable to LIBs is described.

2.3. Ultrasonic testing

US testing is a well established method of monitoring solid bodies through the use of high-frequency sound waves, and is very sensitive to surface and subsurface discontinuities. Sound is the oscillation of pressure through a host medium. When travelling through a medium, the wave dissipates energy via attenuation. Attenuation is the loss of acoustic energy via reflection and absorption, where the acoustic energy is converted into thermal energy within a medium [48]. At an interface between two mediums, such as a crack in a steel block or an iron plate in contact with a copper plate, the wave can be reflected, absorbed or transmitted. This allows for real-time monitoring of material properties, flaw detection and evaluation, and changes in material dimensions [49]. The velocity of a sound wave, c (m s^{-1}), depends on the medium density and elastic modulus, given by:

$$c = \sqrt{E/\rho} \tag{1}$$

where E (MPa) is the elastic modulus of the material and ρ (kg m^{-3}) is the material density. If the speed of sound through a material is known, the depth of a discontinuity or a material can be calculated based on the relationship between distance, speed and time. This is known as the time-of-flight (ToF) method.

The acoustic impedance z (Pa s m^{-3}) of a material is the ratio of acoustic pressure within a medium to the velocity of the particles, caused by the sound wave. It is defined as the product of the material density and the sound wave velocity:

$$z = \rho c \tag{2}$$

When an US wave reaches an interface between two media, some of the wave is reflected and part is transmitted into the new medium. The proportion of the wave reflected at the interface is called the reflection coefficient, R. The reflection coefficient is defined using the acoustic impedances of the two materials, given in Eq. (3):

$$R = (z_2 - z_1)/(z_2 + z_1) \tag{3}$$

where z_1 and z_2 are the acoustic impedances of the primary and secondary material [50]. As Eq. (3) shows, the materials with similar acoustic impedances will transmit a larger proportion of the wave compared to materials that have differing acoustic impedances, such as air and steel. A sound wave is produced by a piezoelectric transducer, which generates US waves – when subjected to an electrical current – and injects them into the sample.

There are two main inspection modes for US: pulse-echo and pitch-catch [51,52]. The pulse-echo mode is a one transducer setup in which the transducer emits and receives the US signal in order to investigate the reflections from discontinuities or boundaries. Pulse-echo ultrasound is commonly used for medical purposes [53,54] and non-destructive testing [55,56]. The pitch-catch mode is a multi-transducer setup in which two identical transducers are mounted on the material. One transducer acts as the emitter, whilst the other acts as the receiver. This arrangement removes the noise generated by the initial pulse by preventing oscillation interference [57]. The transducers are usually placed on the same face. To ensure the receiving sensor detects the wave, the pulse is emitted at an angle. The transducers can also be located directly opposite one another, referred to as the through-pulse mode. This setup is also useful for non-destructive testing, such as the structural health of cylindrical pipes [58] and metallic joining technologies [59]. The pitch-catch mode has also been sued for 3D imaging [60]. See Fig. 1 for a visualisation of the three modes. Such modes can be used for SOC and SOH monitoring in LIBs, as the movement of Li-ions would change the material properties of the electrodes, thereby changing the acoustic signal. This is further explored in Section 3.1.1.

3. Literature review

In this section, Section 3.1 will define the hardware used and the mechanics of US, and specify how it can be utilised for LIB monitoring, and explore the use of US to monitor the SOC and SOH of LIBs. Section 3.2 reviews work done on TR in LIBs, categorised by abuse case: overheating; penetration; overcharging; and gas generation. Current methods of detecting TR are discussed at the end of the section in order to evaluate their performance against ultrasonic detection of TR, which is discussed in Section 3.3. This section also looks at work performed on testing the viability of US on monitoring LIBs under abuse conditions, such as increased operating temperatures and over-charging.

3.1. Ultrasonic monitoring of state-of-charge and state-of-health in Li-ion batteries

The SOC, and by extension SOH, can be measured by the change in voltage, charge, and temperature of the cell as stated in Section 2.2. Voltage and charge data provide insight into the cell; however, it does not provide the greatest accuracy for the SOC of the cell. The

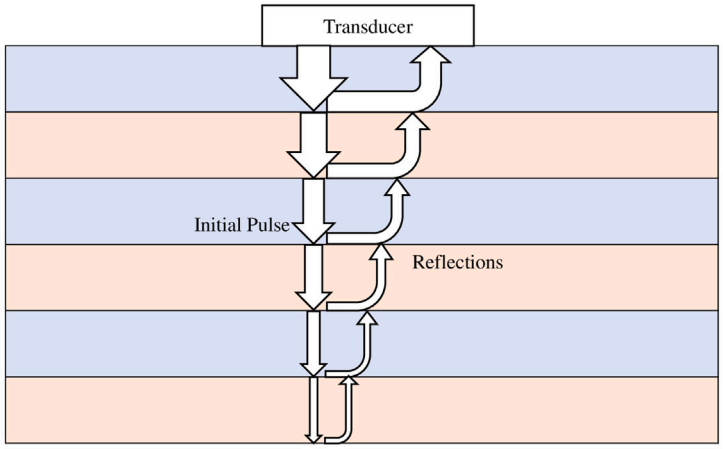

(a) Pulse-echo.

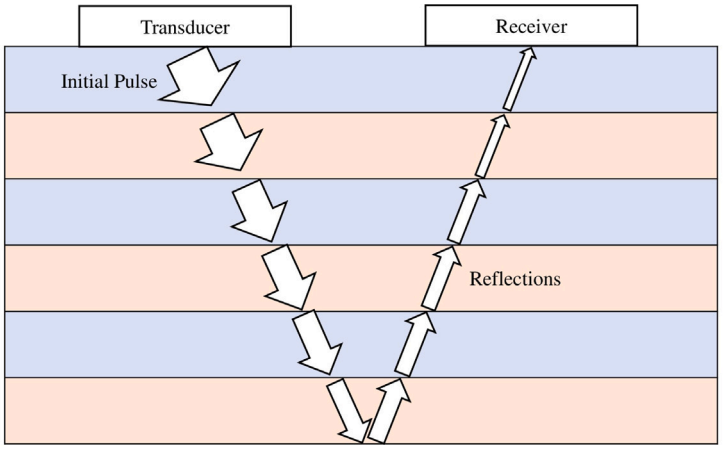

(b) Pitch-catch.

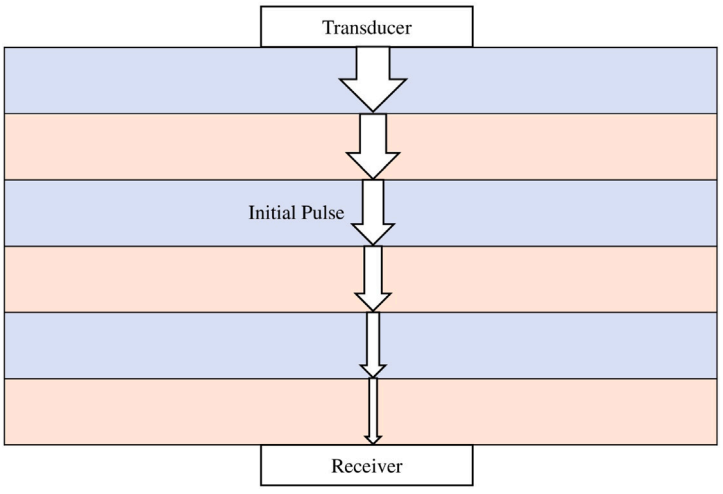

(c) Through-pulse.

Fig. 1. Sketch of how acoustic signals travel are recorded by transducers in the (a) pulse-echo mode, (b) pitch-catch mode and (c) through-pulse mode. The sketches shows a single interaction at each interface, where the signal is part transmitted and part reflected. However, this would occur multiple times, causing interference resulting in a complex signal of multiple reflections. This is not an issue for the through-pulse mode, as the pulse does not cross an interface more than once.

parameters used are measured outside the cell; they are the outputs of the change in SOC. Temperature data provides limited insight into the state of safety (SOS) of the cell, and therefore of the potential of thermal runaway [61]. Temperature does not provide SOC information by itself however.

US has been implemented to provide insight into the SOC and SOH of LIBs. The SOC is measurable due to density and stiffness changes within the electrodes due to lithium intercalation/deintercalation [62]. This results in a speed of sound change in the electrodes, see Eq. (1). The ToF will be affected by the change in speed of sound, allowing the SOC to be monitored [11]. As this method is based on internal changes to the cell, US can provide a different perspective to conventional BMSs. Combining these methods could create a more complete view of the cell/pack in question and improve the accuracy of the estimation.

Cell degradation is measurable due to the gas generation, electrode expansion, residual stress development or electrode ruffling/delamination. As these modes appear and progress, the cell will swell. This increases the distance the US wave must travel, resulting in a change in ToF. The US wave will also attenuate at a greater rate in an older battery as a result of these modes: gas will create more interfaces within the cell that have high reflection coefficients; electrode ruffling/delamination leads to less contact between the electrodes, reducing the transmissibility of the wave. These result in a weaker signal [10].

3.1.1. Ultrasonic setup and battery hardware

US monitoring of LIBs is a non-destructive method, allowing for *in-situ* testing. The hardware required for US testing consists of a piezoelectric ceramic element, either directly bonded to the cell or held in contact with the cell in a casing, which is called a contact probe. If bonded directly, a thin layer of adhesive is used to secure the transducer to the cell. If within a housing, a thin layer of US gel is applied between the cell surface and the transducer in order to improve the coupling between the transducer and cell [63].

As stated in Section 2.3, the most common modes are pitch-catch and pulse-echo. This is performed with either a contact probe, or with directly bonded piezoelectric elements. These are usually used to monitor changes in the SOC during non-abusive cycling, as well as cell degradation during both abusive and non-abusive cycling. Other arrangements have been used to monitor LIBs, such as an air coupled setup [64]. Air coupled methods involve a through-pulse mode where the elements are not in contact with the sample; the wave will travel through the air before and after travelling through the cell.

In literature there has been a range of frequencies tested, from 200 kHz to 5 MHz; laboratory use-cases tend to higher frequencies and closer-to-application uses tend to lower frequencies [10,11,65–67]. The frequency of the wave is limited by the resolution and penetration of the pulse [68], where the resolution refers to the timing between the discrete measurements used to describe the reflection signals. For example, a resolution of 12.8 ns for a measurement of 6 μs, would result in 495 discrete measurements.

The penetration refers to how deep into the sample the US wave can travel before it fully attenuates. At each medium interface, part of the wave is reflected, part is transmitted and part is absorbed. The frequency has an effect on the penetration power of a wave; a higher frequency will have less penetration power but greater sensitivity. Finding a compromise between sensitivity and penetration is important to gain the most information about the cell without large signal attenuation. The information is collected from an amplitude scan (Ascan). An AScan shows the change in amplitude of the signal over time. A high amplitude signal relates to a strong reflection, and a low amplitude signal relates to a weak reflection. A reflection refers to the acoustic energy exciting the receiving transducer. The number of peaks do not correlate to the number of layers; a peak is not representative of a single layer, but the culmination of many reflections from within the cell.

If a pulse-echo mode is used, the AScan consists of the generated pulse and the reflections. A pitch-catch or through-pulse would not have the generated pulse visible in the AScan. When utilising the pitch-catch mode, the received signal ensures all active layers of the battery have been monitored — the signal would not otherwise be received. A full battery diagnosis and charge monitor of the battery is therefore possible. However, a more complex system is required for operation. In contrast, the pulse-echo mode does not ensure full battery diagnosis, as the penetration depth of the signal cannot be confirmed. This could call into question the bias of the signal between temperature and charge [5].

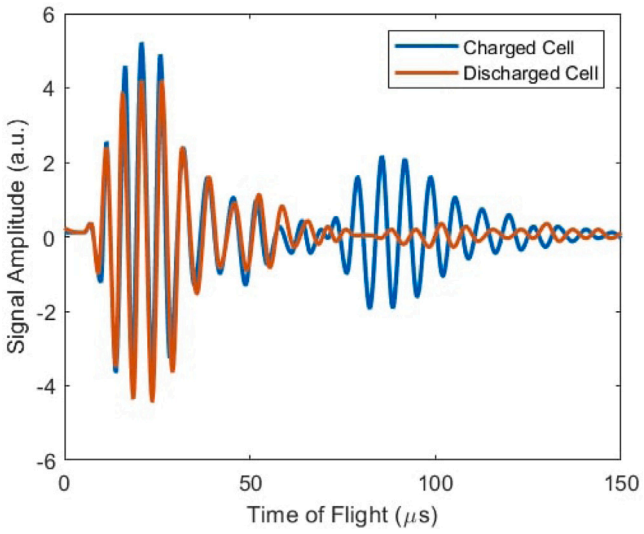

Fig. 2. AScan of 200 kHz pulse through a cell at fully charged and fully discharged states.
Source: Recreated from [65].

3.1.2. SOC monitoring

The method used to infer SOC in LIBs via US is based on the principle that the movement of Li-ions during charge/discharge leads to a change in density, and in turn the acoustic impedance, of the electrodes. As described in Eq. (3), the proportion of the signal that is reflected will therefore vary. The distribution of Li-ions, along with the rate of change of the distribution, could provide insight in to the SOH. The cell chemistry would not have an effect on the adaptability of this method as the movement of the ions is integral to the operation of the cells.

The first paper showing the application of US ToF to monitor the SOC and SOH of batteries was written by Hsieh et al. in 2015 [11]. In this paper, two 2.25 MHz sensors were placed in a through-pulse setup. The cells were $LiCoO_2$/graphite prismatic pouch cells. Alongside this, the pulsing sensor listening for the response, in a pulse-echo setup. It was found that the ToF peak shifts towards lower values and the signal increased in intensity during charging. The opposite was true for discharging; the ToF shift would tend towards higher values and the signal intensity would decrease.

Gold et al. [65] used US testing to validate the determination of SOC based on volumetric expansion of the graphite. It was found that 200 kHz was the most favourable and allowed for easy discrimination between charged and discharged states. This difference can be seen in Fig. 2. It was found that the second reflection has a ToF shift of ~30 μs between charged and discharged. The signal amplitude demonstrated a relation to the SOC; the first reflection was unaffected by the change in SOC, but the second reflection showed a linear reduction in amplitude of 14.08±0.61% as the cell was discharged. The authors concluded that the SOC can be determined without a reference electrode. Therefore, the SOC of LIBs could be estimated using the direct US method in real-use cases.

It was unknown from Gold's research what dependencies the US signal had when estimating the SOC. To address this, Popp et al. [69] investigated the effects of C-rate and temperature on the measured ToF. They found that the C-rate produced uncertainties in the ToF measurements, with higher C-rates resulting in longer ToF and less pronounced local minima. This behaviour was possibly influenced by inhomogeneity in the Li-ion distribution in the electrodes [70]. Higher temperatures resulted in a higher ToF, due to the decreased stiffness of the cell at higher temperature, and thus a lower wave propagation speed. As expected, the ToF also varied with the SOC, as at 25 °C, the change in ToF between charged and discharged was 10 μs.

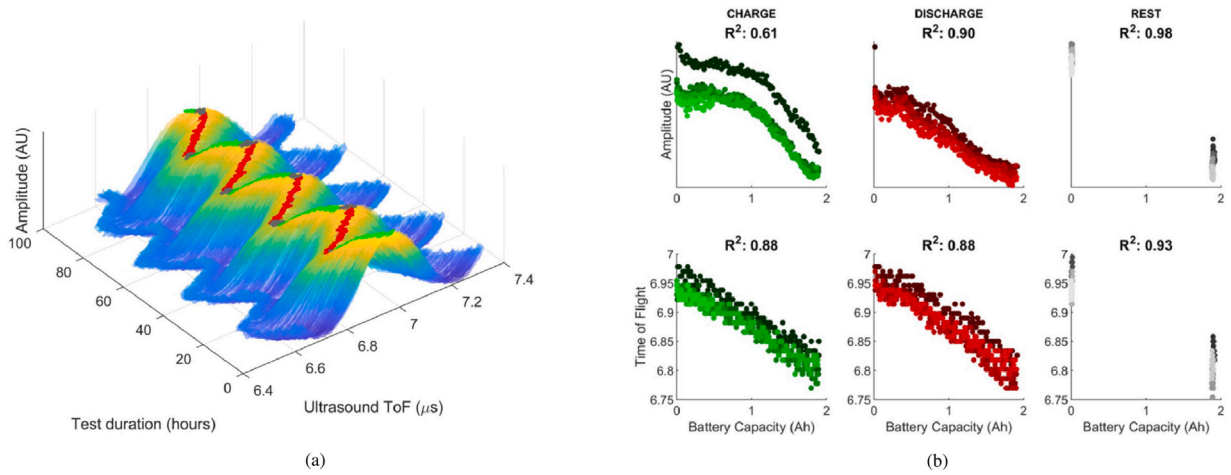

Fig. 3. (a) Graphical peak evolution throughout a charging test (b) the correlation plots of the charge states with amplitude and ToF [5].

The literature described used longitudinal US waves; there are multiple types of US propagation types. One of these types is surface – or Rayleigh – waves, which were investigated by Ladpli et al. [71]. It was found that they were able to estimate the SOH and SOC with error less than 0.05% and 0.36%, respectively. Surface waves differ from other US waves as they travel across the surface of a medium, rather than penetrating into the medium. The penetration of surface waves is dependent on the wavelength [72], thereby reducing the ability to monitor changes in the electrode layers deeper within the cell.

A non-contact method was tested, where the 400 kHz sensors were situated 40 mm from the cell, suspended in the air. The SOC estimation was possible even with the low signal-to-noise ratio present in the test. A near linear relationship was also stated to exist between the amplitudes of both the longitudinal wave and the SOC [64].

Copley et al. [5] studied the qualities in a signal passing through the different layers of a LIB. A model was developed to understand the features and nature of the US signal, and validated against a repeat experiment of Hsieh et al. [11]. The model indicated that small changes to the electrode properties, such as density and elastic modulus, could have a significant effect on the US signal. ToF shift had a stable correlation with the charge state of the cell, whereas the amplitude was found to be unstable. Fig. 3 shows that the ToF correlation is consistent for both charge and discharge, but the amplitude varies between the two states. Frequency was suspected to have an effect on signal reliability; if the wave has weak penetrating power, then the signal is dominated by layers close to the sensor and are susceptible to temperature bias.

Multiple chemistries have been tested, including LCO and LFP [73]. LFP cells were shown to have a lower SOC estimation error, of 1%, compared to LCO, of 2.3 to 3%, when using ToF and signal amplitude. This was an improvement over using voltage measurements; LFP had an error of 6% and LCO had an error of 3%. This suggests that the cathode chemistry has an effect of the reliability of US monitoring. The authors did not provide a suggestion as to why there is a difference in accuracy. A possible explanation for this could be the change in cathode mechanical properties during battery operation. As defined in Eqs. (1) and (3), the elastic modulus and density of the cathodes will affect the speed of sound and attenuation of the signal. A smaller change in elastic modulus will result in a smaller change in speed of sound resulting in a smaller ΔToF available to use for SOC estimation. Further testing is required to determine this discrepancy.

Table 2 summarises the research and respective findings in this subsection.

3.1.3. SOH monitoring

Sood et al. [10] used two 5 MHz transducers in a pitch-catch mode and cycled the cells to investigate signs of cell degradation. The ultrasonic response was used to monitor swelling, electrode expansion, electrode ruffling, delamination and voiding within a LIB. The LIB was put through numerous charge cycles, and a change in the AScan signal was detected. The weakened signal was concluded to be from degradation, though the cause of said degradation was not determined. The cause of the degradation was suspected to be gas evolution, residual stress on the interfaces or electrode expansion.

Rather than looking at detecting degradation methods, Ladpli et al. [74] used guided-wave-based US waves to monitor the change in ToF during artificial aging of LIBs using bonded piezoelectric transducers. The results, shown in Fig. 4 a, demonstrate a decrease in ToF as a battery ages. This contradicts the results found by Wu et al. [75] (see Fig. 4 b) where it was found that the deviation of the increased ToF becomes more prominent as the cell ages. The cause of this increased ToF is a result of the density changes of the electrodes, as the Li-ion content in each electrode changes as the cell charges and discharges. A Spearman coefficient greater than 0.94 was calculated showing a high correlation between ToF and SOH [75]. In the over-charge test, the authors found that the ToF increased sharply after some time (2.8 h). The authors suggested the over-charging caused internal gas generation, which resulted in cell expansion.

Oca et al. [76] studied Li-ion capacitors abused by mild over- and under-charge. The capacitors were rated to 2.2–3.8 V, with the mild under-charge/over-charge defined as 2.0 V and 4.5 V, respectively. They found ToF can be used to detect permanent changes that may not be seen from voltage alone. They state that ToF is a good indicator of swelling, initiated during discharge over the first mild over-charge, which agrees Wu et al. [75]. However, they were unable to determine whether the ToF change was due to change in the electrode material or gas generation.

Bommier et al. [77] studied SEI formation within NMC - Si/graphite cells as well as long-term cycling effects. The cells were instrumented with two 2.25 MHz transducers in a through-pulse mode. It was found that the onset of gassing – suggested to be caused by the initial formation of the SEI – was detected by a loss in acoustic signal. This was only present in cells with Si/graphite anodes [11]. As the cell was cycled and the capacity drop increased, an upward ToF trend was found.

Robinson et al. [78] used a 5 MHz sensor in 36 locations to spatially resolve US diagnostics of the electrodes in LIBs. The authors state that the acoustic peaks were typically doublets, or two peaks in close proximity. These doublets exhibited a noticeable change during charging and discharging: during charging the earlier peak would decrease in amplitude whilst the later peak would increase in amplitude. This was attributed to the density changes in the anodes and cathodes, with one peak associated to one electrode type. The depth of the anode current

Table 2
Table of SOC diagnosis using ultrasound.

Aim	Diagnosis	Transducer setup	Reference
Through-pulse measurements of SOC and SOH using ToF	ToF had an inverse linear relationship with SOC	2.25 MHz contact probe 200 kHz Bonded transducer	[11] [65]
	Linear relation between signal amplitude and SOC	125 kHz Air-coupled through-pulse	[64]
C-rate and temperature effects on ToF	Relationship between increased C-rate and ToF and temperature and ToF	25–40 kHz surface waves	[69]
Through-pulse measurements of SOC and SOH using ToF	Low error estimation of SOC and SOH, despite shallow penetration	Surface-wave pitch-catch	[71]
Model ToF changes based on electrode property changes	ToF has consistent correlation with SOC	Model	[5]

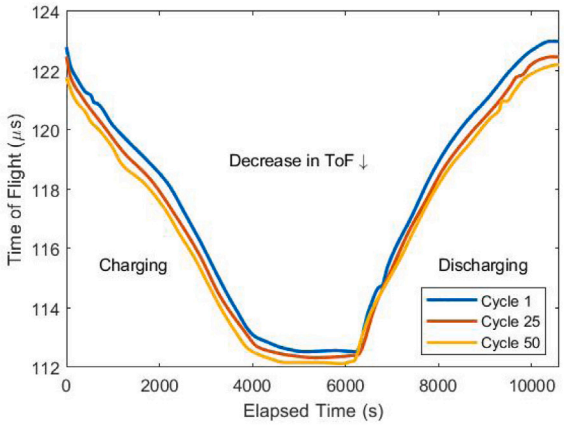

(a) US Spectra demonstrating the change in ToF during a full charge and discharge cycle for a single AScan peak. A comparison between different cycles shows a general decrease in ToF as the cell aged. Recreated from [74].

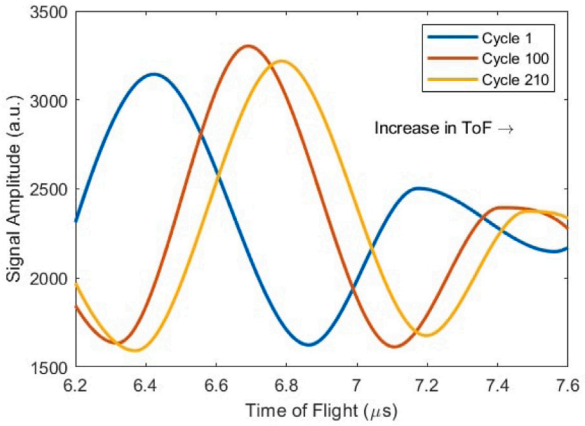

(b) First reflection of an AScan after different charge cycles. An increase in ToF can be seen by the shift of the first peak to the right, but the rate of change of ToF decreases as the cell is further cycled. A change in amplitude of the peaks is also observed. Recreated from [75].

Fig. 4. Comparison of ToF change of a single AScan peak from two cells during aging testing.

collecting tab was detected due to variation in the ToF across the 36 locations. This suggests that localised defects could be detected using ultrasound.

In order to test this, the viability of detecting defects within Li-ion cells using US was investigated by Robinson et al. [79]. Bespoke pouch cells of pristine condition and built-in defects were compared. The defects were accurately measured and verified, in terms of location/depth and scale, via the use of X-ray tomography. It was found that the signal must be tailored to the cell. A microscale defect was also recorded, that was ca. 20 μm in diameter. An area of 200 μm around the defect was observed in a commercial cell to create an acoustically resistive 'void', affecting the propagation pathway. This resulted in a delayed response in the signal, which was not detected in the bespoke cells.

Table 3 summarises the research and respective findings in this subsection.

3.1.4. Summary

Recent research had suggested that US monitoring of LIBs could be used to infer the SOC and SOH of cells despite it being an emerging field. It has been posited that information regarding the internal conditions of cells could be provided without damaging the cells. The technique could also be used in tandem with conventional BMSs to provide a more concrete understanding of cells. However, use of US to identify and decouple the failure modes in LIBs requires further work.

It is difficult to identify features within a cell as the US signal is complex due to the culmination of the main pulse and smaller internal reflections. It is suggested that defects and degradation could be detected, and characterised by depth and size, using US. But the failure mechanism/mechanisms causing the degradation were not discernable without the use of other techniques. This also means multiple defects could not be separated from each other, as the effects would be combined within the US signal.

Ultrasonic monitoring of LIBs is subject to limitations. Notably, as the monitored cell experiences degradation or develops defects, the ultrasonic signal response undergoes analogous changes, such as a global ToF shift [74,75]. Such changes can have an adverse effect on the precision of SOC estimations, as this is reliant on the shift in ToF.

There are some disagreements in the literature; for example, the ageing of a cell has been shown to both increase and decrease the ToF. The cause of this discrepancy could be the behaviour exhibited by the cell as it ages; gas generation would reduce the acoustic signal and SEI formation would increase the ToF due to an increased path length — the SEI formation creates new layers within the cell [77]. Further research is required to decouple gas generation, electrode delamination, voiding and electrode expansion such that the effects due to aging can be isolated.

The impact of temperature on ToF measurements is a subject of debate within the literature. Preliminary research has suggested that temperature may have a reduced effect on ToF within earlier ranges (up to 5 μs) [4], though modelling data argues that temperature variation could reduce the reliability of the US signal [5]. Further investigation is imperative to determine the influence of temperature, both in static and dynamic states, on US measurements conducted at varying ToF ranges.

3.2. Thermal runaway

Thermal runaway is a significant safety concern for LIBs as it can lead to a fire and/or an explosion [80,81]. The occurrence of TR events are rare, but as the use of LIBs increases it is important to develop technologies that prevent TR and allow detection in its earliest stages. There are two practical detection methods that can be incorporated

Table 3
Table of SOH diagnosis using ultrasound.

Aim	Diagnosis	Transducer setup	Reference
Detection of degradation methods	Amplitude decreased as the cell was cycled	5 MHz pitch-catch	[10]
ToF shift during cell ageing	ToF decreases as cell ages ToF increases as the cell ages	Guided-wave pitch-catch 1 MHz pulse-echo	[74] [75]
Capacitor degradation during over- and undercharge	ToF shifts could be used to detect gas swelling and SOC changes	125–500 kHz through-pulse	[76]
US detection of SEI formation and cycle-induced capacity loss	Onset of gassing from SEI formation was detected by the ToF. ToF increased as capacity dropped	2.25 MHz through-pulse	[77]
Spatial resolution of electrodes	ToF shifts agreed with previous reports. Able to detect the depth of the anode current collecting tab.	5 MHz pulse-echo	[78]
Detection of localised defects in cells	Defects were measured and verified	10 MHz pulse-echo	[79]

Table 4
Summary of the events during thermal runaway and their respective onset temperatures.

Feature	Expected value	Reference
Swelling/delamination	40 °C/60 °C	[84]
SEI decomposition	57 °C[a], 80 °C[b]	[15,92]
Electrolyte evaporation	60–100 °C	[93]
Anode decomposition	80–160 °C	[94–97]
Separator melt (PE/PP)	130 °C /170 °C	[81]
Onset of self-heating	0.02 °C min^{-1}	[98]
Onset of Thermal runaway	1.0 °C min^{-1}	[98]

[a] Theoretical.
[b] Detectable.

into LIBs for the early detection of TR onset. These are expansion (dilatometry, strain/force) and acoustic (acoustic emission, US probing) based methods [67].

TR within a LIB is a process in which the exothermic chemical decomposition of the active battery materials and electrolyte lead to exponentially increasing reaction and heat generation rates with temperature [82,83]. Failure within LIBs leading to TR can be caused by thermal (e.g. cell overheating), physical (e.g. cell penetration) and electrical (cell over-charge) abuse. During failure, multiple events occur including: cell swelling [84]; SEI decomposition; gas generation; the separator melting; electrolyte evaporation; internal short-circuiting and; cathode–electrolyte interaction [15,81–83,85–91]. See Table 4 for the expected temperatures and temperature rates of the events stated, which is visualised in Fig. 5 along with the effects from over- and under-charging.

3.2.1. Thermal abuse

LIBs have an optimum operating temperature of 20 °C to 40 °C [99]. Outside this range, the battery experiences accelerated aging [100]. The increased aging is caused by the buildup of the SEI, increasing the internal resistance of LIBs. The SEI is the decomposition of the active electrode materials and conductive salt within the interface between the separator and the active electrodes [101]. The chemistry of the cathode and SOC of the cell both affect the thermal stability (i.e. onset of thermal decomposition) and heat released during TR, shown in Table 5 [83,102–105].

LFP cells tested under adiabatic calorimetry in an accelerated rate calorimeter (ARC) were observed to not undergo TR below 28% SOC, but at SOC greater than 28% TR onset occurred at approximately 200 °C. as seen in Fig. 6. The anode was the major influence on self-heating in the cell at an SOC above 28% up to 100%, above which the cathode and anode have more equal influence [98]. This has been explained as a fully lithiated anode generates an order of magnitude more heat than a fully lithiated cathode [91,97].

LCO cells have been observed to have poorer thermal stability than LFP cells. At 50% and 100% SOC, the LCO cells were found to have a much greater explosive power than the LFP cells, reaching an equivalent of 1.77 g of TNT at 100% SOC [115]. The TNT equivalents can be seen in Table 6. Though it should be noted that while both chemistries exhibited high temperatures and pressures, LCO cells exhibited greater temperatures and pressures.

Table 5
Reaction properties of different cathode materials [106].

Cathode	Ref.	Temperature range of decomposition (°C)	Heat release (J g^{-1})
LCO	[107]	220–500	450
NCA	[108]	160	850 ± 100
	[109]	200	793
LMO	[110]	225–400	350 ± 100
	[107]	150–300	450
	[111]	89	2014.3
LFP	[112]	190–285	290
	[113]	180	145
NCM	[114]	17	322.7
	[114]	178	364.3
	[114]	183	534.6
	[114]	199	645.8

Table 6
TNT equivalent of cells at thermal runaway [115].

Cathode material	SOC (%)	TNT equivalent (g)
LFP	50	0.11
LFP	100	0.23
LCO	50	0.88
LCO	100	1.77

Compared to LCO, LMO exhibit a greater thermal stability across all SOC up to 120%. This was examined by Hernandez et al. [104]. Two types of 18 650 cells, one LCO and one LMO, were charged to the desired SOC, then placed in an ARC. The cells were heated using a Heat-Wait-Seek (HWS) method, which heated the cells by 5 °C with a waiting-step of 30 min and a seeking-step of 5 min. The seeking step monitored for high self-heating rates, defined as above 0.05 °C min^{-1}. As stated, LCO cells undergo TR at 50% SOC and above. LMO cells undergo TR at 75% SOC and above, with consistently lower temperature increase rates compared to LCO cells, as seen in Fig. 7 [104].

Synthesised $LiMnPO_4$ (LMP) cells have been found to be less thermally stable than LFP cells, as greater amounts of heat are produced when overheated at a delithiated state. This is accompanied by a lower onset temperature on par with NCA cells [90,116].

3.2.2. Mechanical abuse

Penetration induced TR in an array of NMC cells was investigated by Feng et al. [82]. The first battery was penetrated by a nail to a depth of 8 mm at a speed of 10 mm/s. From penetration, it took around 10 s for the penetrated cell to reach TR, with the following cells reaching TR due to the heat from their respective preceding cell.

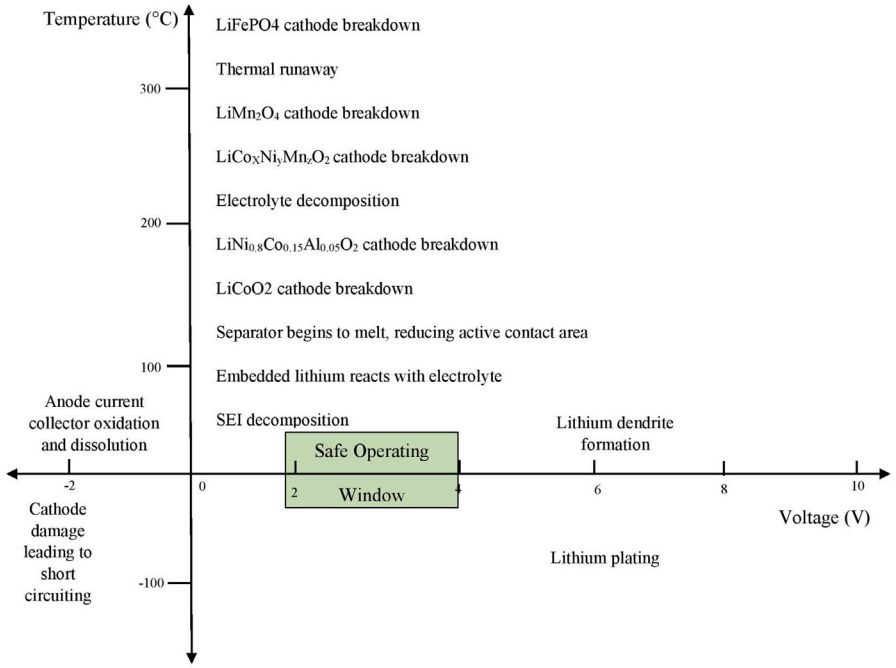

Fig. 5. Generalised safe operating range of Li-ion cells, and events that occur outside said range.
Source: Recreated from [12].

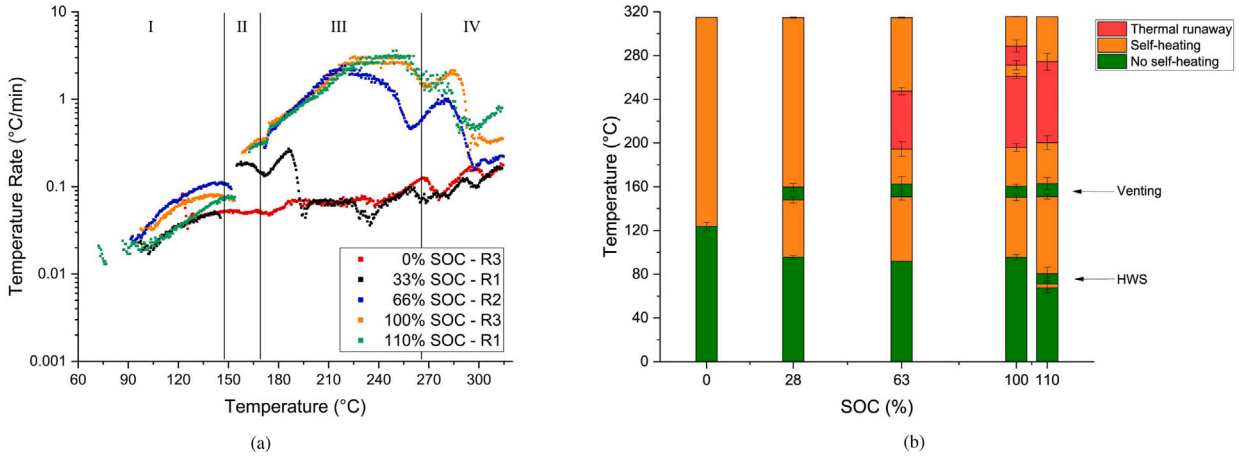

Fig. 6. (a) Rate of temperature change of LFP cells at different states-of-charge within an ARC. (b) Thermal map of (a) stating when a cell underwent self-heating and entered thermal runaway at the tested states-of-charge.
Source: Reproduced from [98].

Once TR was achieved, it took around five seconds for the sixth cell to reach TR. It was found that the TR onset temperature was lower for penetration than for uniform heating TR. The cause of TR was the breakdown of the separator, causing short circuiting [82,117]. However when penetrated, the temperature distribution through the cells is not uniform, as the heat generation localises around the penetrated area. This creates a temperature variation throughout the cell. The TR propagation is independent of fire during the self-heating, as the heat transfer between the cells had little variation from the cells that caught fire and those that did not [118].

The thermal and electrochemical behaviour of a penetrated cell is independent of the penetration speed [119,120]. The location of the nail when penetrating had an effect on the thermal behaviour. Penetration at the edge of the electrode was found to be more dangerous, as the heat dissipation to the cell wall/nail is limited by the separator and electrolyte thermal conductivity [121]. The SOC of the cell had an effect on the onset of TR, similar to [98]. For 18 650 cells with cathode material of 98% NMC and 2% LMO, an SOC of less than 50% would not lead to TR when the cell is penetrated, which was found to be higher than the cutoff for uniform thermal heating of 28%. The maximum temperature of the cell was also dependent on the SOC: a higher SOC results in a higher TR maximum temperature [122].

3.2.3. Electrical abuse

Over-charging-induced TR is dangerous due to the excess energy in the cell [81,123]. When the SOC of the cell is charged above 120%, oxidation within the electrolyte occurs, and lithium deposition on the anode surface begins [124,125]. The SEI film would thicken due to a solvent reaction with the deposited lithium, increasing the internal resistance [125]. Above an SOC of 140%, the cell would see an increase in the rate of temperature rise causing: swelling; increased electrolyte oxidation and heat generation [126,127]. This would cause the SEI to decompose, leading to an lithiated anode–electrolyte reaction [82,94]. There was a drop in voltage, despite the SOC increasing [31]. Above

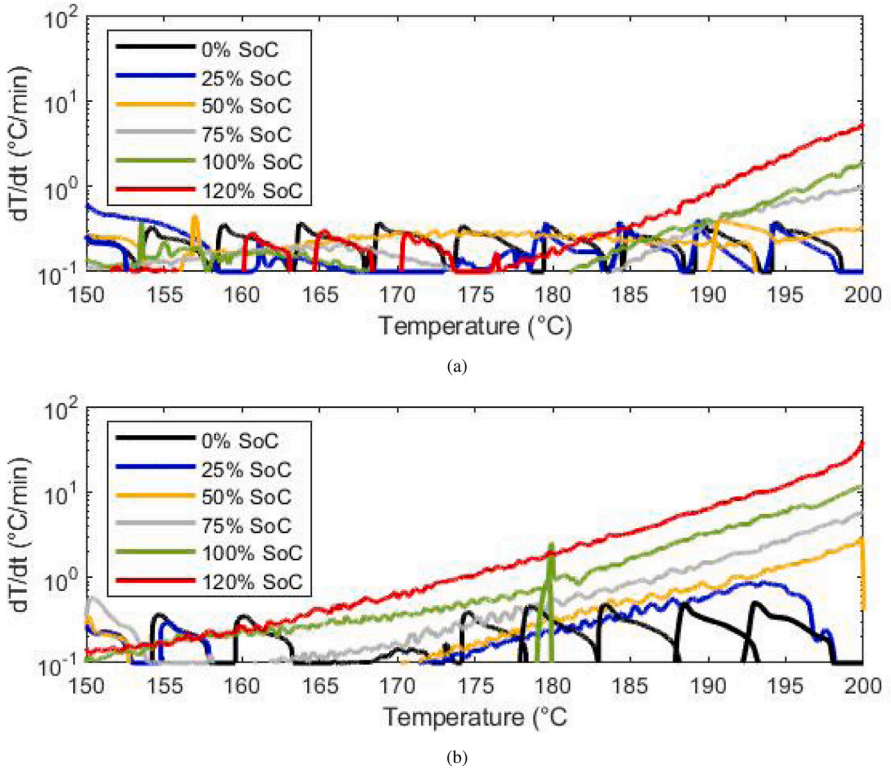

Fig. 7. Heating rate compared to temperature of a (a) LMO cell and a (b) LCO cell at various states-of-charge.
Source: Recreated from [104].

160% SOC, the internal pressure ruptures the cell, leading to thermal runaway [126].

The heat generation caused by over-charging was investigated by Saito et al. [128], where it was found the heat generation was closely proportional to the charging current. This suggests the heat generation is largely influenced by ohmic heating. The onset of heating was located in the cathode, regardless of the cathode lithiation [129]. The cathode also provides the strongest intensity of TR when heated, compared to the other materials in the cell [130]. When a cell has been over-charged, a number of outcomes can occur; the cell can swell from gas generation at low currents and rupture at higher currents [129].

The effect of over-charging on the onset of TR was investigated by Zhang et al. [131]. The cells were charged to SOCs of 100%, 105%, 110%, 115%, 120% then heated via HWS. The cells were measured for the self heating temperature, T1 (self-heating rate of > 0.02 ° C min^{-1}), TR trigger temperature, T2 (> 5 °C min^{-1}) and maximum temperature, T3. It is shown that the TR onset temperature decreases with SOC increase above 100%. It was stated that the time required to reach TR also decreases up to 4.8 V, suggesting that over-charging can cause an early onset of TR [131,132].

3.2.4. Gas generation

Gas generation occurs during normal and abusive operation of LIBs. Monitoring the gas production internally within a cell is challenging with typical state determination methods derived from voltage, current and temperature measurements [133,134]. However, mechanical measurements could provide information about internal condition of cells, specifically regarding to safety, as they can detect the physical changes resulting from decomposition [67].

The evolution of gases during lithium-ion operation is not fully understood. During normal operation, multiple gases are generated due to chemical reactions. One such gas is C_2H_4. During the first cycle, there is a sharp increase in concentration in C_2H_4. The formation of the SEI layer is suggested to be associated with this generation [135,136]. Following the initial formation, concentration of C_2H_4 gas increases at a slower rate, independent of the cycling voltage [136] or stops increasing [137]. CO is believed to evolve simultaneously with C_2H_4, but can be attributed to the absorbed-on-cathode atomic oxygen during electrolyte decomposition [138]. Increase in the concentration of CO_2 rise is believed to be a result of a chemical reaction between residual moisture and CO evolution on the anode during the charge cycle [137]. H_2 evolution is believed to be the result of residual H_2O in the cell [138,139]. A comprehensive review of gas generation and evolution during normal operation is covered by Rowden et al. [136].

The generation of gases can cause internal structural changes and delamination when a cell is heated above normal operating temperatures. Gas pockets have been seen using CT and X-ray imaging when the surface temperature reached values greater than 100 ° C [87,140]. Over-charging a LCO pouch cell showed that swelling began at 40 °C with no adverse changes to the voltage profile, while delamination was observed at 60 °C with a rise in voltage as internal resistance increased due to gas generation and delamination [84]. Compared to temperature rate data [82,83] this shows that gassing occurs before significant rates are recorded, and hence provides an opportunity for the early detection of TR. In these cases, gas was generated from the decomposition/degradation of the electrolytes and SEI, which can be a result of both thermal and electrical abuse.

NMC cells have a similar thermal stability to LCO, as at 50% SOC the cells do not undergo TR [141]. This was observed using force readings, along with temperature and voltage readings similar to the methods mentioned above. Notably, for both 50% and 100% SOC, there was an abrupt and substantial rise in force readings, followed by a subsequent decline. This observed pattern exhibited a strong association with the generation and subsequent venting of gases. The rate of gas generation was found to be faster at higher SOC than lower SOC, and this was observed in the force readings [141].

Swelling is not uncommon to observe in abused Li-ion pouch cells. The swelling increases the stress on the cell casing and internal layers

Table 7
Evaluation of different sensors based on three criteria. Signal clarity describes how close the detection signal comes to a step function and how easy it is to evaluate it, whereas sensor feasibility evaluates how easy the sensor can be deployed.
Source: Reproduced from [147].

Sensor	Detection speed	Signal clarity	Sensor feasibility
S1 — voltage	Bad	Good	Good
S2 — gas	Good	Good	Bad
S3 — smoke	Bad	Neutral	Neutral
S4 — creep	Bad	Bad	Good
S5 — temperature	Neutral	Neutral	Neutral
S6 — pressure	Good	Bad	Good
S7 — force	Good	Bad	Neutral

leading to cell rupture and delamination, respectively [142,143]. The delamination of the internal layers in the jelly roll of hard cased cells (cylindrical and prismatic) is caused by the gas generation, along with the heat generation [87,123]. The gas will also increase the overall thermal resistance of the cell significantly [143,144]. This is due to the increased spacing between the layers, where the initial thermal resistance of the air is negligible compared to the layers.

3.2.5. Detection of TR

Failure mechanisms can be present in the lead up to TR, such as gas generation; temperature increase; and voltage drop. In order to detect TR, monitoring attempts of these mechanisms have been made.

As stated in Section 3.2.4, gas generation occurs before changes in temperature. Modelling the efficacy of gas generation monitoring as a TR detection method has been performed by Cai et al. [145]. Nine NMC 18 650 cells were modelled in a three by three grid in the centre of a cylindrical drum with a radius of 0.292 m and a height of 0.85 m. The centre cell was externally short circuited and underwent TR. The drum was modelled at atmospheric CO_2 concentrations – 400 ppm – and would detect TR at a CO_2 concentration of 2000 ppm. The time taken for the neighbouring cells to undergo TR was 710 s, called t_{crit}. The gas sensors detected TR after 85 s, which was significantly quicker than t_{crit}. At t_{crit}, the drum surface temperature changed by less than 0.001 °C.

Force sensors have also been used to measure gas generation during TR. A cell was fixed in place, with force sensors attached to the corners of the fixture in order to measure battery expansion [141]. Two NMC pouch cells underwent internal short circuiting, one at 50% SOC and one at 100% SOC. Only the 100% SOC cell underwent TR. However, the force sensors were able to detect internal cell pressures for both tests accurately when compared to the modelled pressure increase. Both tests saw a quick drop in force, which was due to the cells venting.

Attempts to use temperature for TR onset detection have been made. External surface temperature measurements were unable to provide enough time in order to shut off the cell before TR and more extreme reactions, such as fires, could occur [146].

Seven sensors – voltage; gas; smoke; temperature; pressure; creep; and force – were tested and compared by Koch et al. [147]. Three experiments, V1; V2; and V3, involved cells undergoing TR. V1 was an NMC cell that underwent thermally induced TR. V2 and V3 involved multiple NMC cells undergoing penetration induced TR. The capacity of the cells differed between tests, but were consistent within each test. The sensors were based on three criteria: detection speed; signal clarity; and sensor feasibility. Each sensor was graded good, neutral or bad for these criteria, see Table 7 for performance in these criteria. It was found that no single method was deemed the 'favourite'.

In a similar fashion, Klink et al. [148] compared seven detection sensors. These were: voltage; current; temperature; strain; gas; smoke; and pressure. A model-based method was also compared. The experimental methods were all capable of detecting TR more than five minutes before TR onset, which was the baseline for the work. The model was the quickest in detecting TR; TR was detected significantly prior to the five minute pre-warning time. The smoke and gas sensors also achieved this. There were eight criteria the sensors were tested on: detection time; certainty; localisation; monitoring; complexity; integration; scalability; and transferability. The model performed the best against these criteria, with voltage, gas and smoke performing the best out of the experimental methods. This is in disagreement with Koch et al. as the smoke sensor did not perform as well in their work [147]. Further investigation is required to conclude the effectiveness of these sensors. There was contention over the efficacy of the gas sensor. Koch et al. stated that the gas sensor is not feasible given the large size and energy requirement [147], while Klink et al. stated that it is a viable method [148]. Both papers were in agreement of the feasibility of the other sensors.

3.2.6. Summary

Li-ion cells can be damaged by multiple abuse mechanisms, including thermal, mechanical and electrical. These mechanisms can cause failure mechanisms such as: electrode delamination; electrode decomposition; short circuiting; gas generation; and cell self heating, all which can lead to thermal runaway. The chemistry and SOC of the cell has also been shown to have an effect on the behaviour of TR, including the onset of TR and the overall hazards from the failed cell. Research into the detection of TR is limited, and not always successful [149].

Multiple sensors for detecting TR have been tested including gas, temperature, voltage, smoke, and force [145–148]. Not all these methods were able to detect TR individually, but were successful when combinations of the sensors were used. The gas sensor was shown to have good detection speed and signal clarity across multiple tests, however there is contention with the feasibility of such a sensor [147,148]. Current BMS struggle to monitor gas production [133,134]. US has been shown to be sensitive to internal changes within cells in Section 3.1.3, such as gas generation [79], whilst having a smaller form factor and lower power consumption, which may make it a viable method of detecting TR.

3.3. Ultrasonic monitoring of Li-ion abuse and thermal runaway

As shown in Section 3.1, US monitoring of LIBs has been a growing field in the last decade. While Section 3.2 showed that TR monitoring of Li-ion batteries has been a large field for over a decade. However, there has been little work that considers coupling these two research areas which together have the potential to make significant advancements in the detection of TR. However, interest in coupling these two areas have developed in recent years.

In 2019, Robinson et al. [4] looked into the cycling behaviour of LIBs using US, and assessed the impact of thermal expansion caused by temperature change during charging. A 210 mA h LCO cell was cycled at 1 C, with the US data at 25 °C and 30 °C being recorded. The cell was then heated in a climate-controlled environment, with the US data being recorded at the temperature extremes. From the AScans of the climate-controlled tests it was observed that there were no significant changes in the low ToF peaks (0 to 5 us). However small changes in the signal amplitude were observed; the 30 °C signal had a slightly greater amplitude over the 25 °C signal for most of the peaks. The authors suggested the change in intensity was due to variations in the Young's modulus rather than temperature.

Chang et al. [150] cycled LCO cells over a temperature range of 0 - 60 °C. Using US, it was demonstrated that the cells underwent catastrophic failure across the temperature range. Lithium plating typically occurs below 10 °C with this cathode, which can lead to excessive gassing if a high temperature shift occurs. In order to monitor this, cells were cycled at 1 C at temperatures below 10 °C then heated to 20 ° C, 30 °C, 40 °C, 50 °C and 60 °C . It was found that for all tests, the ToF shifted after cycling and heating, with the shift increasing in magnitude with temperature. All tests also saw a loss in acoustic signal. The 60 °C test saw signal loss within one hour of reaching the target temperature

and the 20 °C test losing acoustic signal after approximately 63 h of reaching the target temperature. This was suggested to be caused by accelerated electrolyte degradation at higher temperatures, combined with the lithium plating.

Zappen et al. [100] measured in-plane and through plane signals during the thermal abuse of a pouch cell. The cell was heated with pauses until 110 °C, at which point it was allowed to passively cool. When plotting the US signal amplitude against temperature, changes in the signal were identified at 65 °C and then again at 90 °C. This is in the temperature range of SEI decomposition and electrolytes evaporation. Unlike other work, Zappen used the *centre of gravity* (μs) of the US signal to infer material changes. The *centre of gravity* is dependent on the speed of sound through the medium as well as the signal intensity. For both the signal intensity and *centre of gravity*, there was a significant change at 90 °C. The signal intensity reduced while the centre of gravity increased for both in-plane and through-plane readings.

Pham et al. [143] investigated gas-induced delamination during thermal runaway using US. A trend of increased ToF was observed during gradual cell heating, which was attributed to the decrease in density of the electrodes, leading to a decrease in propagation speed. The rate of heating, and therefore the rate of propagation of thermal runaway, had a positive affect on the ToF shift; a more gradual propagation resulted in a more gradual ToF shift. A gradual thermal runaway propagation also led to prolonged gas generation, which meant a greater time between the loss of the US signal and the onset of thermal runaway. The test used two 210 mA h cells. Cell 1 underwent gradual heating, whilst cell 2 underwent more aggressive heating. The more gradual heating of cell 1 resulted in a sharper increase in ToF and a more abrupt loss of signal compared to cell 2, yet the onset of failure began later. It was suggested that the quicker propagation of TR in cell 1 was due to the lower temperature gradient, resulting in a higher average temperature.

Owen et al. [151] looked into the behaviour of US signals based on changes in temperature and charge cycling rates. It was found that, at constant SOC, the ToF increased as the temperature increased, with the shift becoming greater at lower SOC. This was measured over a range of 0 to 10 μs, focusing on the first echo around 8 to 9 μs. The relationship between temperature and ToF was linear across all SOC, as well as the gradient of temperature and SOC. The authors also looked into decoupling the temperature effect on ToF from the SOC. This was achieved by subtracting the change in ToF caused by temperature change – from a separate test – from the measured change in ToF from the charge cycle. The difference between the corrected and measured ToF was shown to diverge more as the temperature increased during discharge, suggesting temperature has an effect on the change in ToF shown in Fig. 8. The resultant shifts in ToF were suggested to be due to material changes of the electrodes as they "relaxed", as indicated by a similar change in the voltage.

Appleberry et al. [152] used pitch-catch US monitoring to provide warnings about cell over-charging, and test feasibility of stopping cell operation (E-stop). The warnings would occur if the signal amplitude would reduce by at least 3.5 standard deviations from normal operation, and the cell would stop when the amplitude dropped below 10 standard deviations. The US detection consistently identified failure conditions as each test resulted in a warning and a triggered E-stop. Time before warning and E-stops did vary between the tests (see Table 8.) At the point of these warning the signal amplitude decreased rapidly. The loss of amplitude was attributed to the gas generation from the overcharge scenario.

4. Discussion and recommendations

US monitoring of the Li-ion cells has been researched and implemented in literature. Either by direct coupling or air coupling, the SOC of cells can be accurately estimated over a large range of frequencies. The sensors are low cost and easy to implement onto current cells,

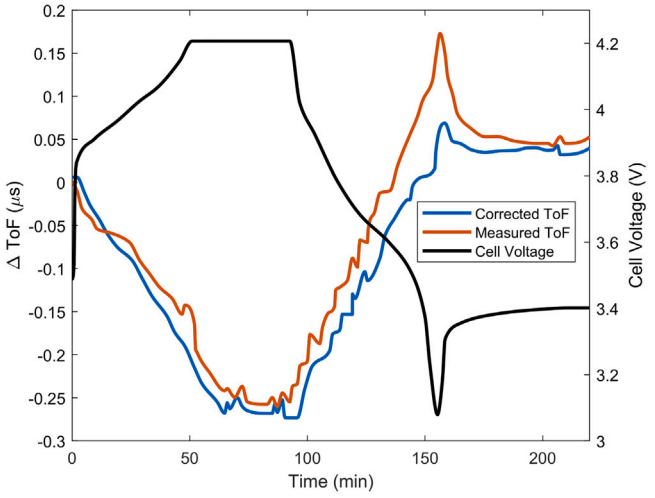

Fig. 8. Difference in ToF variation due to temperature effects, superimposed on the voltage profile.
Source: Adapted from [151].

however the form factor of many sensors used are too large for non-academic applications. Individual transducers, which have a small form factor, have been successfully used at low frequency. Pitch-catch and pulse-echo inspection modes have both proven effective at monitoring LIBs. The benefit of this approach is the ability to measure the internal failure mechanisms of the cell *in-situ*, allowing for the detection of gas generation, swelling, lithium-plating and aging of cells in a non-destructive method. Detection of these behaviours can occur much earlier using US compared to more conventional BMS systems. While research has shown the aforementioned failure mechanisms can be detected in dedicated failure tests, further work is required to identify which failure mode is occurring within a cell under real world operating conditions. Considering that failure modes of this type can occur simultaneously there is also the need to deconvolute the signals of concurrent failures so that the correct failure mechanism is identified.

Abuse conditions have been widely studied in LIBs as a result of the inherent risks of this technology, notably the risk of thermal runaway. The cathode material has a major effect on the stability of the cell, causing the onset of TR to vary across LIBs. Independent variables in the cell, such as the SOC, C-rate and temperature, also have an effect on the stability of the cell. The monitoring of TR can be detected when the cell is electrically, thermally or mechanically abused. The cause of internal gas generation, and subsequent cell swelling, has been researched in different chemistries and cell form factors. However, the detection of TR is still needing development, as these methods require external variables to monitor the cell. External variables include, but not limited to, open-circuit voltage characterisation and Coulomb counting. Open-circuit voltage characterisation requires cutting off power to the cell to allow for an extended period of rest, meaning it is not applicable for *in-situ* use [153]. Coulomb counting requires knowledge of the initial SOC and cell capacity, and is at risk of errors such as time oscillation drift [154]. The use of a BMS with the addition of US sensors to monitor the internal and external behaviours of cells could improve the detection of abuse symptoms, allowing for the mitigation of thermal runaway during cell operation.

Recently research has begun into the use of US to monitor temperature and TR effects in LIBs. Symptoms of abuse conditions can be detected by US signals during thermal and electrical abuse testing. The coupling of the temperature and SOC effects on the US signal is an aspect that needs addressing in order to allow this application of US to be accurate. Ref. [4] determined that temperature did not have an effect on the US signal within 5 μs, as the difference in the AScans

Table 8
Summary of experiments and the respective response time for the warning and E-stop compared to the failure time.
Source: Reproduced from [152].

Experiment	Induced failure	Warning before failure	E-Stop before failure	Time from overcharge to failure
1	~23 °C, CC-overcharge	124 min (81%)	54 min (35%)	154 min
2	~23 °C, CC-overcharge	90 min (66%)	90 min (66%)	136 min
3	~23 °C, CV-overcharge	93 min (93%)	92 min (92%)	100 min
4	~23 °C, CV-overcharge	348 min (99%)	347 min (99%)	352 min
5	65 °C, CV-overcharge	21 min (84%)	15 min (60%)	25 min
6	65 °C, CV-overcharge	20 min (65%)	19 min (61%)	31 min
7	65 °C, CV-overcharge	12 min (75%)	4 min (25%)	16 min
8	65 °C, CC-overcharge	76 min (50%)	58 min (38%)	151 min
9	65 °C, CC-overcharge	285 min (99%)	139 min (48%)	289 min

at 25 °C and 30/°C showed slight variation but was suggested to be caused by differences in the elastic modulus. However, refs [5,151] found that when charging/discharging, the temperature, and rate of change, causes the US signal to deviate from the expected result outside of 5 μs. During operation, cells generate heat energy due to internal resistance. This heat energy causes thermal expansion in all layers of the cell, increasing the volume of the cell. This results in a longer US path, and therefore longer ToF. Thermal expansion also increases the speed of sound (see Eq. (1)) which would decrease the ToF. Additional to these thermal effects, the (de)intercalation of lithium-ions within the electrodes and their movement through the cell will change the elastic modulus, density and volumes of all layers, thereby affecting the speed of sound and ToF. As shown by [151], temperature has an overall increase in ToF. This suggests that the thermal expansion of the cell has a greater effect than the density change due to temperature and the change in material properties due to (de)intercalation.

To address the need for temperature-charge decoupling some methods are proposed to determine the relationships.

1. Measure and compare the ToF and temperature of a cell that has undergone two cycles: a charge cycle; and a thermal cycle — where a cell is externally heated up and cooled at a constant SOC. By matching the temperatures of both cycles, the hysteresis between the two signals would allow for the effects of temperature and charging to be decoupled.
2. Thermally cycle a cell at various SOC in steps, in a manner similar to [151], in order to look for deviations in the ToF across temperature and SOC. By isolating the change in SOC and temperature, comparisons of ToF at a constant SOC across different temperatures or vice-versa can be made.

5. Conclusion

This article provides a review of using US in LIB state monitoring and thermal behaviour. First, literature covering the various estimation methods regarding state-of-charge and state-of-health was analysed, discussing the findings noting disagreements or gaps in the research such as: the change in ToF due to cell aging; and the degree that temperature changes the acoustic response. Next, the article presented an analysis of abuse cases in Li-ion batteries. The literature was categorised by abuse case, exploring the causes for each case and their respective progression to thermal runaway. Next, several academic sources exploring the application of US for abuse monitoring/thermal runaway prevention were presented, along with the effect of temperature and charge on the US signal.

This work shows that US has been shown to detect internal changes within Li-ion batteries, however there is a need for research into: the identification and characterisation of individual internal defects without the aid of other techniques; the decoupling of temperature and charge effects on the US signal. US can detect internal changes/defects, and is able to characterise them by size and depth, but cannot determine what said change is without the use of supplementary equipment. Multiple defects within a single cell cannot be individually characterised, as the AScan will show the resultant effect of the combined defects.

Additionally, this review found the temperature-charge relationship with the US signal needs to be decoupled in order to increase the efficacy of estimating the state-of-charge and to assist in thermal runaway detection. There is contention around the effect of temperature on the ToF when measuring the SOC in the earlier ToF ranges (0 to 5 μs), but at later ranges it has been found that there is a greater impact from temperature. The decoupling of temperature and charge has been started, but further tests need to be performed in order to confirm the usability of decoupling. This could be done by: comparing the ToF hysteresis between a charge cycle and thermal cycle or; look for deviations in the ToF for a thermally cycled cell at multiple SOC.

CRediT authorship contribution statement

Daniel Williams: Writing – original draft, Visualization, Writing – review & editing. **Royce Copley:** Conceptualization, Writing – original draft. **Peter Bugryniec:** Writing – review & editing, Visualization. **Rob Dwyer-Joyce:** Supervision, Writing – review & editing. **Solomon Brown:** Conceptualization , Supervision, Writing – review & editing.

Declaration of competing interest

The authors declare that they have no known competing financial interests or personal relationships that could have appeared to influence the work reported in this paper.

Data availability

No data was used for the research described in the article.

Funding

The fourth author was supported by the Centre for Doctoral Training in Integrated Tribology EP/L01629X/1. The third and last author were supported by the Faraday Institution, UK [grant number FIRG028].

References

[1] B. Nykvist, M. Nilsson, Rapidly falling costs of battery packs for electric vehicles, Nature Clim. Change 5 (2015) http://dx.doi.org/10.1038/nclimate2564.
[2] Y. Ding, Z.P. Cano, A. Yu, J. Lu, Z. Chen, Automotive li-ion batteries: Current status and future perspectives, Nat. Clim. Electrochem. Energy Rev. 2 (2019) http://dx.doi.org/10.1007/s41918-018-0022-z.
[3] T.A. Faunce, J. Prest, D. Su, S. Hearne, F. Iacopi, On-grid batteries for large-scale energy storage: Challenges and opportunities for policy and technology, MRS Energy Sustain. 5 (10) (2018) http://dx.doi.org/10.1557/mre.2018.11.
[4] J.B. Robinson, M. Pham, M.D.R. Kok, T.M.M. Heenan, D.J.L. Brett, P.R. Shearing, Examining the cycling behaviour of Li-Ion batteries using ultrasonic time-of-flight measurements, J. Power Sources 444 (2019) http://dx.doi.org/10.1016/j.jpowsour.2019.227318.

[5] R. Copley, D. Cumming, Y. Wu, R. Dwyer-Joyce, Measurements and modelling of the response of an ultrasonic pulse to a lithium-ion battery as a precursor for state of charge estimation, J. Energy Storage 36 (2021) http://dx.doi.org/10.1016/j.est.2021.102406.

[6] J. Wen, Y. Yu, C. Chen, A review on lithium-ion batteries safety issues: Existing problems and possible solutions, Mater. Express 2 (3) (2012) http://dx.doi.org/10.1166/mex.2012.1075.

[7] C. Jhu, Y. Wang, C. Wen, C. Shu, Thermal runaway potential of $LiCoO_2$ and $Li(Ni_{1/3}Co_{1/3}Mn_{1/3})O_2$ batteries determined with adiabatic calorimetry methodology, Appl. Energy 100 (2012) http://dx.doi.org/10.1016/j.apenergy.2012.05.064.

[8] K. Qian, Y. Li, Y. He, D. Liu, Y. Zheng, D. Luo, B. Li, F. Kang, Abuse tolerance behavior of layered oxide-based Li-ion battery during overcharge and over-discharge, RSC Adv. 80 (2016) http://dx.doi.org/10.1039/C6RA11288A.

[9] T. Yokoshima, D. Mukoyama, F. Maeda, T. Osaka, T. K, S. Egusa, S. Naoi, S. Ishikura, K. Yamamoto, Direct observation of internal state of thermal runaway in lithium ion battery during nail-penetration test, J. Power Sources 393 (2018) http://dx.doi.org/10.1016/j.jpowsour.2018.04.092.

[10] B. Sood, M. Osterman, M. Pecht, Health monitoring of lithium-ion batteries, in: 2013 IEEE Symposium on Product Compliance Engineering, ISPCE, IEEE, 2013, http://dx.doi.org/10.1109/ispce.2013.6664165.

[11] A.G. Hsieh, S. Bhadra, B.J. Hertzberg, P.J. Gjeltema, A. Goy, J.W. Fleischer, D.A. Steingart, Electrochemical-acoustic time of flight: in operando correlation of physical dynamics with battery charge and health, Energy Environ. Sci. 8 (5) (2015) http://dx.doi.org/10.1039/c5ee00111k.

[12] L. Lu, X. Han, J. Li, J. Hua, M. Ouyang, A review on the key issues for lithium-ion battery management in electric vehicles, J. Power Sources 226 (2013) http://dx.doi.org/10.1016/j.jpowsour.2012.10.060.

[13] C.A. Zamai, D. Bavoso, A.A. Rodrigues, J.A.S. Barbosa, Sistema de gestión de carga para baterías de ion-litio, Pontifical Javeriana University, 2018, URL http://repository.javeriana.edu.co/handle/10554/21433.

[14] K. Edström, M. Herstedt, D.P. Abraham, A new look at the solid electrolyte interphase on graphite anodes in Li-ion batteries, J. Power Sources 153 (2) (2006) http://dx.doi.org/10.1016/j.jpowsour.2005.05.062.

[15] R. Spotnitz, J. Franklin, Abuse behavior of high-power, lithium-ion cells, J. Power Sources 113 (1) (2003) http://dx.doi.org/10.1016/S0378-7753(02)00488-3.

[16] H. Lin, D. Chua, M. Salomon, H. Shiao, M. Hendrickson, E. PLichta, S. Slane, Low temperature behaviour of Li-ion cells, Electrochem. Solid-State Lett. 4 (2001) http://dx.doi.org/10.1149/1.1368736.

[17] S. Wang, K. Rafiz, J. Liu, J. Lin, Effects of lithium dendrites on thermal runaway and gassing of $LiFePO_4$ batteries, Sustain. Energy Fuels 4 (2020) http://dx.doi.org/10.1039/d0se00027b.

[18] W. Lu, C. López, N. Liu, J. Vaughey, A. Jansen, D. Dees, Overcharge effect on morphology and structure of carbon electrodes for lithium-ion batteries, J. Electrochem. Soc. 159 (2012) http://dx.doi.org/10.1149/2.jes035205.

[19] T. Langner, T. Sieber, J. Acker, Studies on the deposition of copper in lithium-ion batteries during the deep discharge process, Sci. Rep. 11 (6316) (2021) http://dx.doi.org/10.1038/s41598-021-85575-x.

[20] C. Fear, D. Juarez-Robles, J. Jeevarajan, P. Mukherjee, Elucidating copper dissolution phenomenon in Li-ion cells under overdischarge extremes, J. Electrochem. Soc. 165 (2018) http://dx.doi.org/10.1149/2.0671809jes.

[21] J. Duan, X. Tang, H. Dai, Y. Yang, W. Wu, X. Wei, Y. Huang, Building safe lithium-ion batteries for electric vehicles, Electrochem. Energy Rev. 3 (2019) http://dx.doi.org/10.1007/s41918-019-00060-4.

[22] X. Feng, D. Ren, X. He, M. Ouyang, Mitigating thermal runaway of lithium-ion batteries, Joule 4 (2020) http://dx.doi.org/10.1016/j.joule.2020.02.010.

[23] V. Pop, H.J. Bergveld, P.H.L. Notten, P.P.L. Regtien, State-of-the-art of battery state-of-charge determination, Meas. Sci. Technol. 16 (2005) http://dx.doi.org/10.1088/0957-0233/16/12/R01.

[24] M.A. Hannan, M.S.H. Lipu, A. Hussain, A. Mohamed, A review of lithium-ion battery state of charge estimation and management system in electric vehicle applications: Challenges and recommendations, Renew. Sustain. Energy Rev. 78 (2017) http://dx.doi.org/10.1016/j.rser.2017.05.001.

[25] J. Rivera-Barrera, N. Muñoz-Galeano, H. Sarmiento-Maldonado, SoC estimation for lithium-ion batteries: Review and future challenges, Electronics 102 (6) (2017) http://dx.doi.org/10.3390/electronics6040102.

[26] B. balasingam, M. Ahmed, K. Pattipati, Battery management systems - Challenges and some solutions, Energies 13 (2020) http://dx.doi.org/10.3390/en13112825.

[27] K.W.E. Cheng, B.P. Divakar, H. Wu, K. Ding, H.F. Ho, Battery-management system (BMS) and SOC development for electrical vehicles, IEEE Trans. Veh. Technol. 60 (2015) http://dx.doi.org/10.1109/TVT.2010.2089647.

[28] D. How, M. Hannan, M. Lipu, P. Ker, State of charge estimation for lithium-ion batteries using model-based and data-driven methods: A review, IEEE Access 7 (2019) http://dx.doi.org/10.1109/ACCESS.2019.2942213.

[29] Y. Wang, J. Tian, Z. Sun, L. Wanfg, R. Xu, M. Li, Z. Chen, A comprehensive review of battery modeling and state estimation approaches for advanced battery management systems, Renew. Sustain. Energy Rev. 131 (2020) http://dx.doi.org/10.1016/j.rser.2020.110015.

[30] M.D. amd T.F. Fuller, J. Newman, Modeling of galvanostatic charge and discharge of the lithium/polymer/insertion cell, J. Electrochem. Soc. 140 (6) (1993) http://dx.doi.org/10.1149/1.2221597.

[31] Y. He, F. Ning, Q. Yang, Q. Song, B. Li, F. Su, H. Du, Z. Tang, F. Kang, Structural and thermal stabilities of layered $Li(Ni_{1/3}Co_{1/3}Mn_{1/3})O_2$ materials in 18650 high power batteries, J. Power Sources 196 (2011) http://dx.doi.org/10.1016/j.jpowsour.2012.01.122.

[32] X. Ding, D. Zhang, J. Cheng, B. Wang, P. Luk, An improved thevenin model of lithium-ion battery with high accuracy for electric vehicles, Appl. Energy 254 (2019) http://dx.doi.org/10.1016/j.apenergy.2019.113615.

[33] I. Sadli, M. Urbain, M. Hinaje, J.-P. Maritn, S. Raël, B. Davat, Contributions of fractional differentiation to the modelling of electric double layer capacitance, Energy Convers. Manage. 51 (2010) http://dx.doi.org/10.1016/j.enconman.2010.06.045.

[34] J. Xu, C. Mi, B. Cao, J. Cao, A new method to estimate the state of charge of lithium-ion batteries based on the battery impedance model, J. Power Sources 233 (2013) http://dx.doi.org/10.1016/j.jpowsour.2013.01.094.

[35] E. Chemali, P. kollmeyer, M. Preindl, A. Emadi, State-of-charge estimation of li-ion batteries using deep neural networks: A machine learning approach, J. Power Sources 400 (2018) http://dx.doi.org/10.1016/j.jpowsour.2018.06.104.

[36] J. Xu, C. Mi, B. cao, J. Deng, Z. Chen, S. Li, The state of charge estimation of lithium-ion batteries based on a proportional-integral observer, IEEE Trans. Veh. Technol. 63 (2014) http://dx.doi.org/10.1109/TVT.2013.2287375.

[37] C. Truchot, M.D. andf B.Y. Liaw, State-of-charge estimation and uncertainty for lithium-ion battery strings, Appl. Energy 119 (2014) http://dx.doi.org/10.1016/j.apenergy.2013.12.046.

[38] K. Ng, C. Moo, Y. Chen, Y. Hsieh, Enhanced coulomb counting method for estimating state-of-charge and state-of-health of lithium-ion batteries, Appl. Energy 86 (2009) http://dx.doi.org/10.1016/j.apenergy.2008.11.021.

[39] J. Kim, G. Seo, C. Chun, B. Cho, S. Lee, OCV hysteresis effect-based SOC estimation in extended Kalman filter algorithm for a $LiFePO_4$/C cell, in: 2012 IEEE International Electric Vehicle Conference, 2012, http://dx.doi.org/10.1109/IEVC.2012.6183174.

[40] M. Berecibar, I. Gandiaga, I. Villarereal, N. Omar, J.V. Mierlo, P.V. den Bossche, Critical review of state of health estimation methods of Li-ion batteries for real applications, Renew. Sustain. Energy Rev. 56 (2016) http://dx.doi.org/10.1016/j.rser.2015.11.042.

[41] Y. Xing, W. He, M. Pecht, K. Tsui, State of charge estimation of lithium-ion batteries using the open-circuit voltage at various ambient temperatures, Appl. Energy 113 (2014) http://dx.doi.org/10.1016/j.apenergy.2013.07.008.

[42] L. Ungurean, G. Cârstoiu, M. Micea, V. Groza, Battery state of health estimation: a structured review of models, methods and commercial devices, Int. J. Energy Res. 41 (2017) http://dx.doi.org/10.1002/er.3598.

[43] D. Andre, C. Appel, T. Soczka-Guth, D. Sauer, Advanced mathematical methods of SOC and SOH estimation for lithium-ion batteries, J. Power Sources 224 (2013) http://dx.doi.org/10.1016/j.jpowsour.2012.10.001.

[44] Y. Xing, E. Ma, K. Tsui, M. Pecht, An ensemble model for predicting the remaining useful performance of lithium-ion batteries, Microelectron. Reliab. 53 (2013) http://dx.doi.org/10.1016/j.microrel.2012.12.003.

[45] D. Liu, J. Pang, J. Zhou, Y. Peng, M. Pecht, Prognostics for state of health estimation of lithium-ion batteries based on combination Gaussian process functional regression, Microelectron. Reliab. 4 (2013) http://dx.doi.org/10.1016/j.microrel.2013.03.010.

[46] J. Jiang, C. Zhang, Fundamentals and Applications of Lithium-ion Batteries in Electric Drive Vehicles, first ed., John Wiley & Sons Singapore Pte Ltd, 2017, http://dx.doi.org/10.1002/9781118414798.

[47] R. Xiong, L. Li, J. Tian, Towards a smarter battery management system: A critical review on battery state of health monitoring methods, J. Power Sources 405 (2018) http://dx.doi.org/10.1016/j.jpowsour.2018.10.019.

[48] S. Flax, N. Pelc, G. Glover, F. Gutmann, M. Mclachlan, Spectral characterization and attenuation measurements in ultrasound, Ultrason. Imaging 5 (1983) http://dx.doi.org/10.1016/0161-7346(83)90013-5.

[49] J. Kräutkramer, H. Kräutkramer, Ultrasonic Testing of Materials, third ed., Springer, 2013, http://dx.doi.org/10.1007/978-3-662-02357-0.

[50] H. Tattersall, The ultrasonic pulse-echo technique as applied to adhesion testing, J. Phys. D: Appl. Phys. 819 (6) (1973) http://dx.doi.org/10.1088/0022-3727/6/7/305.

[51] D. Ensminger, L.J. Bond, Ultrasonics: Fundamentals, Technologies, and Applications, CRC Press, 2011, http://dx.doi.org/10.1201/b11173.

[52] M. Barksi, P. Kedziora, A. Muc, P. Romanowicz, Structural health monitoring (SHM) methods in machine design and operation, Arch. Mech. Eng. 61 (2014) http://dx.doi.org/10.2478/meceng-2014-0037.

[53] J. Hunt, M. Arditi, F. Foster, Ultrasound transducers for pulse-echo medical imaging, IEEE Trans. Biomed. Eng. BME-30 (1983) http://dx.doi.org/10.1109/TBME.1983.325150.

[54] G. Ferraioli, V. Kumar, A. Ozturk, K. Nam, C. de Korte, R. Barr, US attenuation for liver fat quantification: An AIUM-RSNA QIBA pulse-echo quantitative ultrasound initiative, Radiology 302 (2022) http://dx.doi.org/10.1109/TBME.1983.325150.

[55] T. Dourado, A. Alvarenga, F. Peters, W. Mansur, R. Costa-Félix, Simultaneous use of pulse-echo and through-transmission methods in determining a combined reflection coefficient, Appl. Acoust. 192 (2022) http://dx.doi.org/10.1016/j.apacoust.2022.108700.

[56] W. Gray, R. Dwyer-Joyce, In-situ measurement of the meniscus at the entry and exit of grease and oil lubricated rolling bearing contacts, Front. Mech. Eng. 8 (2022) http://dx.doi.org/10.3389/fmech.2022.1056950.

[57] J.O. Majasan, J.B. Robinson, R.E. Owen, M. Maier, A.N.P. Radhakrishnan, M. Pham, T.G. Tranter, Y. Zhang, P.R. Shearing, D.J.L. Brett, Recent advances in acoustic diagnostics for electrochemical power systems, J. Phys. 3 (3) (2021) http://dx.doi.org/10.1088/2515-7655/abfb4a.

[58] D. Sen, A. Aghazadeh, A. Mousavi, S. Nagarajaiah, R. Baraniuj, A. Dabak, Data-driven semi-supervised and supervised learning algorithms for health monitoring of pipes, Mech. Syst. Signal Process. 131 (2019) http://dx.doi.org/10.1016/j.ymssp.2019.06.003.

[59] S. Delrue, M. Tabatabaeipour, J. Hettler, K. Van Den Abeele, Applying a nonlinear, pitch-catch, ultrasonic technique for the detection of kissing bonds in friction stir welds, Ultrasonics 68 (2016) http://dx.doi.org/10.1016/j.ultras.2016.02.012.

[60] B. Lindsey, S. Smith, Pitch–catch phase aberration correction of multiple isoplanatic patches for 3-D transcranial ultrasound imaging, IEEE Trans. Ultrason. Ferroelectr. Freq. Control 60 (2013) http://dx.doi.org/10.1109/TUFFC.2013.2590.

[61] E. Cabrera-Castillo, F. Niedermeier, A. Jossen, Calculation of the state of safety (SOS) for lithium ion batteries, J. Power Sources 324 (2016) http://dx.doi.org/10.1016/j.jpowsour.2016.05.068.

[62] R. Fu, M. Xiao, S. Choe, Modeling, validation and analysis of mechanical stress generation and dimension changes of a pouch type high power Li-ion battery, J. Power Sources 224 (2013) http://dx.doi.org/10.1016/j.jpowsour.2012.09.096.

[63] Y. Fang, L. Lin, H. Feng, Z. Lu, G. Emms, Review of the use of air-coupled ultrasonic technologies for nondestructive testing of wood and wood products, Comput. Electron. Agric. 137 (2017) http://dx.doi.org/10.1016/j.compag.2017.03.015.

[64] J. Chang, X. Zeng, T. Wan, Real-time measurements of lithium-ion batteries state-of-charge based on air-coupled ultrasound, AIP Adv. 9 (2019) http://dx.doi.org/10.1063/1.5108873.

[65] L. Gold, T. Bach, W. Virsik, A. Schmitt, J. Müller, T. Staab, G. Sextl, Probing lithium-ion batteries' state-of-charge using ultrasonic transmission – Concept and laboratory testing, J. Power Sources 343 (2017) http://dx.doi.org/10.1016/j.jpowsour.2017.01.090.

[66] Y. Zhang, A. Radhakrishnan, J. Robinson, R.E. Owen, T. Tranter, E. Kendrick, P. Shearing, D. Brett, In situ ultrasound acoustic measurement of the lithium-ion battery electrode drying process, Appl. Mater. Interfaces 13 (2021) http://dx.doi.org/10.1021/acsami.1c10472.

[67] H. Popp, M. Koller, M. Jahn, A. Bergmann, Mechanical methods for state determination of lithium-ion secondary batteries: A review, J. Energy Storage 32 (2020) http://dx.doi.org/10.1016/j.est.2020.101859.

[68] J. Thijssen, G. Weijers, C. de Korte, Objective performance testing and quality assurance of medical ultrasound equipment, Ultrasound Med. Biol. 33 (2007) http://dx.doi.org/10.1016/j.ultrasmedbio.2006.09.006.

[69] H. Popp, M. Koller, S. Keller, G. Glanz, R. Klambauer, A. Bergmann, State estimation approach of lithium-ion batteries by simplified ultrasonic time-of-flight measurement, IEEE Access 7 (2019) http://dx.doi.org/10.1109/access.2019.2955556.

[70] F. Grimsmann, F. Brauchle, T. Gerbert, A. Gruhle, M. Knipper, J. Parisi, Hysteresis and current dependence of the thickness change of lithium-ion cells with graphite anode, J. Energy Storage 12 (2017) http://dx.doi.org/10.1016/j.est.2017.04.006.

[71] P. Ladpli, F. Kopsaftopoulus, F. Chang, Estimating state of charge and health of lithium-ion batteries with guided waves using built-in piezoelectric sensors/actuators, J. Power Sources (2018) http://dx.doi.org/10.1016/j.jpowsour.2018.02.056.

[72] Y. Fan, S. Dixon, R. Edwards, X. Jian, Ultrasonic surface wave propagation and interaction with surface defects on rail track head, NDT and E Int. 40 (2007) http://dx.doi.org/10.1016/j.ndteint.2007.01.008.

[73] G. Davies, K. Knehr, B. van Tassell, T. Hodson, S. Biswas, A. Hsieh, D. Steingart, State of charge and state of health estimation using electrochemical acoustic time of flight analysis, J. Electrochem. Soc. 164 (12) (2017) http://dx.doi.org/10.1149/2.1411712jes.

[74] P. Ladpli, R. Nardari, F. Kopsaftopoulus, Y. Wang, F. Chang, Design of multifunctional structural batteries with health monitoring capabilities, in: European Workshop on Structural Health Monitoring, 2016.

[75] Y. Wu, Y. Wang, W. Yung, M. Pecht, Ultrasonic health monitoring of lithium-ion batteries, Electronics 8 (7) (2019) http://dx.doi.org/10.3390/electronics8070751.

[76] L. Oca, N. Guillet, R. Tessard, U. Iraola, Lithium-ion capacitor safety assessment under electrical abuse tests based on ultrasound characterization and cell opening, J. Energy Storage 23 (2019) http://dx.doi.org/10.1016/j.est.2019.02.033.

[77] C. Bommier, W. Chang, J. Li, S. Biswas, G. Davies, J. Nanda, D. Steingart, Operando acoustic monitoring of SEI formation and long-term cycling in NMC/SiGr composite pouch cells, J. Electrochem. Soc. 167 (2) (2020) http://dx.doi.org/10.1149/1945-7111/ab68d6.

[78] J.B. Robinson, M. Maier, G. Alster, T. Compton, D. Brett, P. Shearing, Spatially resolved ultrasound diagnostics of Li-ion battery electrodes, Phys. Chem. Chem. Phys. 21 (12) (2019) http://dx.doi.org/10.1039/c8cp07098a.

[79] J. Robinson, R. Owen, M. Kok, M. Maier, J. Majasan, M. Braglia, R. Stocker, T. Amietszajew, A. Roberts, R. Bhagat, D. Billsson, J. Olson, J. Park, G. Hinds, A. Tidblad, D. Brett, P. Shearing, Identifying defects in Li-ion cells using ultrasound acoustic measurements, J. Electrochem. Soc. 167 (12) (2020) http://dx.doi.org/10.1149/1945-7111/abb174.

[80] L. Kong, C. Li, J. Jiang, M. Pecht, Li-ion battery fire hazards and safety strategies, Energies 11 (9) (2018) http://dx.doi.org/10.3390/en11092191.

[81] X. Feng, M. Ouyang, X. Liu, L. Lu, Y. Xia, X. He, Thermal runaway mechanism of lithium ion battery for electric vehicles: A review, Energy Storage Mater. 10 (2018) http://dx.doi.org/10.1016/j.ensm.2017.05.013.

[82] X. Feng, M. Fang, X. He, M. Ouyang, L. Lu, H. Wang, M. Zhang, Thermal runaway features of large format prismatic lithium ion battery using extended volume accelerating rate calorimetry, J. Power Sources 255 (2014) http://dx.doi.org/10.1016/j.jpowsour.2014.01.005.

[83] A. Golubkov, D. Fuchs, J. Wagner, H. Wiltsche, C. Stangl, G. Fauler, G. Voitic, A. Thaler, V. Hacker, Thermal-runaway experiments on consumer Li-ion batteries with metal-oxide and olivin-type cathodes, RSC Adv. 4 (2014) http://dx.doi.org/10.1039/C3RA45748F.

[84] D. Finegan, M. Scheel, J. Robinson, B. Tjaden, M.D. Michiel, G. Hinds, D.J.L. Brett, P.R. Shearing, Investigating lithium-ion battery materials during overcharge-induced thermal runaway: an operando and multi-scale X-ray CT study, Phys. Chem. Chem. Phys. 18 (45) (2016) http://dx.doi.org/10.1039/c6cp04251a.

[85] Q. Wang, J. Sun, X. Yao, C. Chen, Thermal behavior of lithiated graphite with electrolyte in lithium-ion batteries, J. Electrochem. Soc. 153 (2006) http://dx.doi.org/10.1149/1.2139955.

[86] D. Abraham, E. Roth, R. Kostecki, K. McCarthy, S. MacLaren, D. Doughty, Diagnostic examination of thermally abused high-power lithium-ion cells, J. Power Sources 161 (2006) http://dx.doi.org/10.1016/j.jpowsour.2006.04.088.

[87] D. Finegan, M. Scheel, J. Robinson, B. Tjaden, I. Hunt, T. Mason, J. Millichamp, M. Di Michiel, G. Offer, G. Hinds, D. Brett, P. Shearing, In-operando high-speed tomography of lithium-ion batteries during thermal runaway, Nature Commun. 6 (1) (2015) http://dx.doi.org/10.1038/ncomms7924.

[88] G. Kim, A. Pesaran, R. Spotnitz, A three-dimensional thermal abuse model for lithium-ion cells, J. Power Sources 170 (2007) http://dx.doi.org/10.1016/j.jpowsour.2007.04.018.

[89] D. Macneil, J. Dahn, Test of reaction kinetics using both differential scanning and accelerating rate calorimetries as applied to the reaction of LixCoO2 in non-aqueous electrolyte, J. Phys. Chem. A 105 (2001) http://dx.doi.org/10.1021/jp001187j.

[90] G. Chen, T. Richardson, Thermal instability of Olivine-type LiMnPO4 cathodes, J. Power Sources 195 (2010) http://dx.doi.org/10.1016/j.jpowsour.2009.08.046.

[91] A. Kvasha, C. Gutiérrez, U. Osa, I. de Meatza, J. Blazquez, H. Macicior, I. Urdampilleta, A comparative study of thermal runaway of commercial lithium ion cells, Energy 159 (2018) http://dx.doi.org/10.1016/j.energy.2018.06.173.

[92] Q. Wang, J. Sun, X. Yao, C. Chen, Thermal stability of $LiPF_6$/EC + DEC electrolyte with charged electrodes for lithium ion batteries, Thermochim. Acta 437 (1) (2005) http://dx.doi.org/10.1016/j.tca.2005.06.010.

[93] S. Liang, W. Yan, X. Wu, Y. Zhang, Y. Zhu, H. Wang, Y. Wu, Gel polymer electrolytes for lithium ion batteries: Fabrication, characterization and performance, Solid State Ion. 318 (2018) http://dx.doi.org/10.1016/j.ssi.2017.12.023.

[94] E.P. Roth, D.H. Doughty, Thermal abuse performance of high-power 18650 Li-ion cells, J. Power Sources 128 (2) (2004) http://dx.doi.org/10.1016/j.jpowsour.2003.09.068.

[95] M.N. Richard, J.R. Dahn, Accelerating rate calorimetry study on the thermal stability of lithium intercalated graphite in electrolyte. II. Modeling the results and predicting differential scanning calorimeter curves, J. Electrochem. Soc. 146 (6) (1999) http://dx.doi.org/10.1149/1.1391894.

[96] D.D. MacNeil, L. Christensen, J. Landucci, J.M. Paulsen, J.R. Dahn, An autocatalytic mechanism for the reaction of Li_xCoO_2 in electrolyte at elevated temperature, J. Electrochem. Soc. 147 (3) (2000) http://dx.doi.org/10.1149/1.1393299.

[97] I. Belharouak, Y.-K. Sun, W. Lu, K. Amine, On the safety of the $Li_4Ti_5O_{12}$/$LiMn_2O_4$ lithium-ion battery system, J. Electrochem. Soc. 154 (2007) http://dx.doi.org/10.1149/1.2783770.

[98] P. Bugryniec, J. Davidson, D. Cumming, S. Brown, Pursuing safer batteries: Thermal abuse of LiFePO4 cells, J. Power Sources 414 (2019) http://dx.doi.org/10.1016/j.jpowsour.2019.01.013.

[99] R. Korthauer, Handbuch Lithium-Ionen-Batterien, first ed., Springer, 2013, http://dx.doi.org/10.1007/978-3-642-30653-2.

[100] H. Zappen, G. Fuchs, A. Gitis, D. Sauer, In-operando impedance spectroscopy and ultrasonic measurements during high-temperature abuse experiments on lithium-ion batteries, Batteries 6 (2) (2020) http://dx.doi.org/10.3390/batteries6020025.

[101] T. Waldmann, M. Wilka, M. Kasper, M. Fleischhammer, M. Wohlfahrt, Temperature dependent ageing mechanisms in lithium-ion batteries -A Post Mortem study, J. Power Sources 262 (2014) http://dx.doi.org/10.1016/j.jpowsour.2014.03.112.

[102] Q. Wang, J. Sun, X. Chen, G. Chu, C. Chen, Effects of solvents and salt on the thermal stability of charged $LiCoO_2$, Mater. Res. Bull. 44 (2009) http://dx.doi.org/10.1016/j.materresbull.2008.07.006.

[103] D. MacNeil, Z. Lu, Z. Chen, J. Dahn, A comparison of the electrode/electrolyte reaction at elevated temperatures for various Li-ion battery cathodes, J. Power Sources 108 (2002) http://dx.doi.org/10.1016/S0378-7753(01)01013-8.

[104] O. Mendoza-Hernandez, H. Ishikawa, Y. Nishikawa, Y. Maruyama, M. Umeda, Cathode material comparison of thermal runaway behavior of Li-ion cells at different state of charges including over charge, J. Power Sources 280 (2015) http://dx.doi.org/10.1016/j.jpowsour.2015.01.143.

[105] P. Peng, F. Jiang, Thermal safety of lithium-ion batteries with various cathode materials: A numerical study, Int. J. Heat Mass Transfer 103 (2016) http://dx.doi.org/10.1016/j.ijheatmasstransfer.2016.07.088.

[106] Q. Wang, B. Mao, S. Stoliarov, J. Sun, A review of lithium ion battery failure mechanisms and fire prevention strategies, Prog. Energy Combust. Sci. 73 (2019) http://dx.doi.org/10.1016/j.pecs.2019.03.002.

[107] P. Biensan, B. Simon, J. Peres, A. de Guibert, M. Broussely, J. Bodet, F. Perton, On safety of lithium-ion batteries, J. Power Sources 81–82 (1999) http://dx.doi.org/10.1016/S0378-7753(99)00135-4.

[108] Y. Wang, J. Jiang, J. Dahn, The reactivity of delithiated $Li(Ni_1/3Co_{1/3}Mn_{1/3})O_2$, $Li(Ni_{0.8}Co_{0.15}Al_{0.05})O_2$ or $LiCoO_2$ with non-aqueous electrolyte, Electrochem. Commun. 9 (2007) http://dx.doi.org/10.1016/j.elecom.2007.07.033.

[109] Y. Huang, Y. Lin, D. Jenkins, N. Chernova, Y. Chung, B. Radhakrishnan, I. Chu, J. Fang, Q. Wang, F. Omenya, S. Ong, M. Whittingham, Thermal stability and reactivity of cathode materials for Li-ion batteries, Appl. Mater. Interfaces 8 (2016) http://dx.doi.org/10.1021/acsami.5b12081.

[110] Z. Zhang, D. Fouchard, J. Rea, Differential scanning calorimetry material studies: implications for the safety of lithium-ion cells, J. Power Sources 70 (1998) http://dx.doi.org/10.1016/S0378-7753(97)02611-6.

[111] Q. Wang, J. Sun, C. Chen, Thermal stability of delithiated $LiMn_2O_4$ with electrolyte for lithium-ion batteries, J. Electrochem. Soc. 154 (2007) http://dx.doi.org/10.1149/1.2433698.

[112] S. Martha, O. Haik, E. Zinigrad, I. Exnar, T. Drezen, J. Miners, D. Aurbach, On the thermal stability of olivine cathode materials for lithium-ion batteries, J. Electrochem. Soc. 158 (2011) http://dx.doi.org/10.1149/1.3622849.

[113] H. Joachin, T. Kaun, K. Zaghib, J. Prakash, Electrochemical and thermal studies of carbon-coated $LiFePO_4$ cathode, J. Electrochem. Soc. 156 (2009) http://dx.doi.org/10.1149/1.3106121.

[114] J. Gong, Q. Wang, J. Sun, Thermal analysis of nickel cobalt lithium manganese with varying nickel content used for lithium ion batteries, Thermochim. Acta 655 (2017) http://dx.doi.org/10.1016/j.tca.2017.06.022.

[115] T. Lu, C. Chang, S. Wu, K. Chen, S. Lin, C. Wen, C. Shu, Thermal hazard evaluations of 18650 lithium-ion batteries by an adiabatic calorimeter, J. Therm. Anal. Calorim. 114 (3) (2013) http://dx.doi.org/10.1007/s10973-013-3137-9.

[116] S. Martha, B. Markovsky, J. Grinblat, Y. Cofer, O. Haik, E.Z. anjd D. Aurbach, T. Drezen, D. Wang, F. Deghenghi, I. Exnar, $LiMnPO_4$ and $LiMn_{0.8}Fe_{0.2}PO_4$ as advanced cathode materials for rechargeable lithium-ion batteries, J. Electrochem. Soc. (2010) http://dx.doi.org/10.1149/MA2010-03/1/376.

[117] C. Lee, S. Lee, M. Tang, P. Chen, In situ monitoring of temperature inside lithium-ion batteries by flexible micro temperature sensors, Sensors 11 (2011) http://dx.doi.org/10.3390/s111009942.

[118] X. Feng, J. Sun, M. Ouyang, F. Wang, X. He, L. Lu, H. Peng, Characterization of penetration induced thermal runaway propagation process within a large format lithium ion battery module, J. Power Sources 275 (2015) http://dx.doi.org/10.1016/j.jpowsour.2014.11.017.

[119] B. Liu, S. Yin, J. Xu, Integrated computation model of lithium-ion battery subject to nail penetration, Appl. Energy 183 (2016) http://dx.doi.org/10.1016/j.apenergy.2016.08.101.

[120] B. Liu, F. Wang, B. Fan, Z. Zhang, F. Pei, Influence of penetration speeds on power Li-ion-cell's safety performance, J. Automot. Saf. Energy 4 (2013).

[121] H. Maleki, J. Howard, Internal short circuit in li-ion cells, J. Power Sources 191 (2009) http://dx.doi.org/10.1016/j.jpowsour.2009.02.0702.

[122] B. Mao, H. Chen, Z. Chi, T. Wu, Q. Wang, Failure mechanism of the lithium ion battery during nail penetration, Int. J. Heat Mass Transfer 122 (2018) http://dx.doi.org/10.1016/j.ijheatmasstransfer.2018.02.036.

[123] J. Liu, Q. Duan, W. Peng, L. Feng, M. Ma, S. Hu, J. Sun, Q. Wang, Slight overcharging cycling failure of commercial lithium-ion battery induced by the jelly roll destruction, Process Saf. Environ. Prot. 160 (2022) http://dx.doi.org/10.1016/j.psep.2022.02.067.

[124] H. Zheng, Q. Sun, G. Liu, X. Song, V. Battaglia, Correlation between dissolution behavior and electrochemical cycling performance for $LiNi_{1/3}Co_{1/3}Mn_{1/3}O_2$-based cells, J. Power Sources 207 (2012) http://dx.doi.org/10.1016/j.jpowsour.2012.01.122.

[125] N. Sharma, V. Peterson, Overcharging a lithium-ion battery: effect on the LixC6 negative electrode determined by in situ neutron diffraction, J. Power Sources 244 (2013) http://dx.doi.org/10.1016/j.jpowsour.2011.08.042.

[126] D. Ren, X. Feng, L. Lu, M. Ouyang, S. Zheng, J. Li, X. He, An electrochemical-thermal coupled overcharge-to-thermal-runaway model for lithium ion battery, J. Power Sources 364 (2017) http://dx.doi.org/10.1016/j.jpowsour.2017.08.035.

[127] K. Kumai, H. Miyashiro, Y. Kobayashi, K. Takei, R. Ishikawa, Gas generation mechanism due to electrolyte decomposition in commercial lithium-ion cell, J. Power Sources 81 (1999) http://dx.doi.org/10.1016/S0378-7753(98)00234-1.

[128] Y. Saito, K. Takano, A. Negishi, Thermal behaviors of lithium-ion cells during overcharge, J. Power Sources 97 (2001) http://dx.doi.org/10.1016/S0378-7753(01)00703-0.

[129] R. Leising, M. Palazzo, E. Takeuchi, K. Takeuchi, Abuse testing of lithium-ion batteries: Characterization of the overcharge reaction of $LiCoO_2$/Graphite cells, J. Electrochem. Soc. 148 (2001) http://dx.doi.org/10.1149/1.1379740.

[130] J. Weng, X. Yang, D. Ouyang, M. Chen, G. Zhang, J. Wang, Comparative study on the transversal/lengthwise thermal failure propagation and heating position effect of lithium-ion batteries, Appl. Energy 255 (2019) http://dx.doi.org/10.1016/j.apenergy.2019.113761.

[131] G. Zhang, X. Wei, S. Chen, J. Zhu, G. Han, X. Tang, W. Hua, H. Dai, J. Ye, Comprehensive investigation of a slight overcharge on degradation and thermal runaway behavior of lithium-ion batteries, ACS Appl. Mater. Interfaces 13 (2021) http://dx.doi.org/10.1021/acsami.1c06029.

[132] J. Liu, Q. Duan, L. Feng, M. Ma, J. Sun, Q. Wang, Capacity fading and thermal stability of $LiNi_xCo_yMn_zO_2$/graphite battery after overcharging, J. Energy Storage 29 (2020) http://dx.doi.org/10.1016/j.est.2020.101397.

[133] T. Cai, S. Pannala, A. Stefanopoulou, J. Siegel, Battery internal short detection methodology using cell swelling measurements, in: 2020 American Control Conference, ACC, 2020, http://dx.doi.org/10.23919/ACC45564.2020.9147956.

[134] H. Gabber, A. Othman, M. Abdussami, Review of Battery Management Systems (BMS) developmentand industrial standards, Technoligies 9 (2021) http://dx.doi.org/10.3390/technologies9020028.

[135] N. Galushkin, N. Yazvinskaya, D. Glaushkin, Mechanism of gases generation during lithium-ion batteries cycling, J. Electrochem. Soc. 166 (2019) http://dx.doi.org/10.1148/radiol.210736.

[136] B. Rowden, N. Garcia-Araez, A review of gas evolution in lithium ion batteries, Energy Rep. 6 (5) (2020) http://dx.doi.org/10.1016/j.egyr.2020.02.022.

[137] M. Metzger, B. Strehle, S. Solchenbach, H. Gasteiger, Origin of H_2 Evolution in LIBs: H_2O reduction vs. Electrolyte oxidation, J. Electrochem. Soc. 162 (5) (2016) http://dx.doi.org/10.1149/2.1151605jes.

[138] R. jung, M. Metzger, F. Maglia, C. Stinner, H. Gasteiger, Oxygen release and its effect on the cycling stability of $LiNi_xMn_yCo_zO_2$ (NMC) cathode materials for Li-ion batteries, J. Electrochem. Soc. 164 (2016) http://dx.doi.org/10.1149/2.0021707jes.

[139] R. bernhard, M. Metzger, H. Gasteiger, Gas evolution at graphite anodes depending on electrolyte water content and SEI quality studied by on-line electrochemical mass spectrometry, J. Electrochem. Soc. 162 (10) (2015) http://dx.doi.org/10.1149/2.0191510jes.

[140] D. Finegan, E. Darcy, M. Keyser, B. Tjaden, T. Heenan, R. Jervis, J. Bailey, N. Vo, O. Magdysyuk, M. Drakopoulos, M. Di Michiel, A. Rack, G. Hinds, D. Brett, P. Shearing, Identifying the cause of rupture of Li-ion batteries during thermal runaway, Adv. Sci. 5 (1) (2018) http://dx.doi.org/10.1002/advs.201700369.

[141] T. Cai, A. Stefanopoulou, J. Siegel, Modeling Li-ion battery temperature and expansion force during the early stages of thermal runaway triggered by internal shorts, J. Electrochem. Soc. (2019) http://dx.doi.org/10.1149/2.1561910jes.

[142] L. Huang, Z. Zhang, Z. Wang, L. Zhang, X. Zhu, D. Dorrell, Thermal runaway behavior during overcharge for large-format lithium-ion batteries with different packaging patterns, J. Power Sources 25 (2019) http://dx.doi.org/10.1016/j.est.2019.100811.

[143] M. Pham, J. Darst, D. Finegan, J. Robinson, T. Heenan, M. Kok, F. Iacoviello, R. Owen, W. Walker, O. Magdysyuk, T. Connolley, E. Darcy, G. Hinds, D. Brett, P. Shearing, Correlative acoustic time-of-flight spectroscopy and X-ray imaging to investigate gas-induced delamination in lithium-ion pouch cells during thermal runaway, J. Power Sources 470 (2020) http://dx.doi.org/10.1016/j.jpowsour.2020.228039.

[144] J. Chen, D. Ren, H. Hsu, L. Wang, X. He, C. Zhang, X. Feng, M. Ouyang, Investigating the thermal runaway features of lithium-ion batteries using a thermal resistance network model, Appl. Energy 295 (2021) http://dx.doi.org/10.1016/j.apenergy.2021.117038.

[145] T. Cai, A. Stefanopoulou, J. Siegel, Early detection for li-ion batteries thermal runaway based on gas sensing, ECS Trans. (2019) http://dx.doi.org/10.1149/08901.0085ecst.

[146] Z. Wei, J. Zhao, H. He, G. Ding, H. Cui, L. Liu, Future smart battery and management: Advanced sensing from external to embedded multi-dimensional measurement, J. Power Sources 489 (2021) http://dx.doi.org/10.1016/j.jpowsour.2021.229462.

[147] S. Koch, K. Birke, R. Kuhn, Fast thermal runaway detection for lithium-ion cells in large scale traction batteries, Batteries (2018) http://dx.doi.org/10.3390/batteries4020016.

[148] J. Klink, A. Hebenbrock, J. Grabow, N. Orazov, U. Nylen, R. benger, H. Beck, Comparison of model-based and sensor-based detection of thermal runaway in li-ion battery modules for automotive application, Batteries 8 (2022) http://dx.doi.org/10.3390/batteries8040034.

[149] M. Tran, A. Mevawalla, A. Aziz, S. Panchal, Y. Xie, M. Fowler, A review of lithium-ion battery thermal runaway modeling and diagnosis approaches, Processes (2022) http://dx.doi.org/10.3390/pr10061192.

[150] W. Chang, C. Bommier, T. Fair, J. Yeung, S. Patil, D. Steingart, Understanding adverse effects of temperature shifts on li-ion batteries: An operando acoustic study, J. Electrochem. Soc. (2020) http://dx.doi.org/10.1149/1945-7111/ab6c56.

[151] R. Owen, J. Robinson, J. Weaving, M. Pham, T. Tranter, T. Neville, D. Billson, M. Braglia, R. Stocker, A. Tidblad, P. Shearing, D. Brett, Operando ultrasonic monitoring of lithium-ion battery temperature and behaviour at different cycling rates and under drive cycle conditions, J. Electrochem. Soc. (2022) http://dx.doi.org/10.1149/1945-7111/ac6833.

[152] M. Appleberry, J. Kowalski, S. Africk, J. Mitchell, T. Ferree, V. Chang, V. Parekh, Z. Xu, Z. Ye, J. Whitacre, S. Murphy, Avoiding thermal runaway in lithium-ion batteries using ultrasound detection of early failure mechanisms, J. Power Sources (2022) http://dx.doi.org/10.1016/j.jpowsour.2022.231423.

[153] R. Xiong, J. Cao, Q. Yu, H. He, F. Sun, Critical review on the battery state of charge estimation methods for electric VEHICLES, IEEE Access 6 (2018) http://dx.doi.org/10.1109/ACCESS.2017.2780258.

[154] K. Movassagh, A. Raihan, B. Balasignam, K. Pattipati, A critical look at Coulomb counting approach for state of charge estimation in batteries, Energies 14 (14) (2021) http://dx.doi.org/10.3390/en14144074.